

Systematic Investigation of the Pr-Ba-Cu-O Phase Diagram

A Dissertation Presented to
the Faculty of the Department of Physics

University of Houston

In Partial Fulfillment
of the Requirements for the Degree
Doctor of Philosophy

By

Lucas Galen Mastalli-Kelly

August 2019

Systematic Investigation of the Pr-Ba-Cu-O Phase Diagram

Luke Mastalli-Kelly

Approved:

Dr. Paul C. W. Chu, Chairman

Dr. Allan J. Jacobson

Dr. Kevin Bassler

Dr. Chin-Sen Ting

Dean, College of Natural Sciences and Mathematics

ACKNOWLEDGEMENTS

Special thanks to Dr. Melissa Gooch for keeping the lab running and many long conversations about this work. Thanks also to Drs. Meen and Jacobson for the chemist's perspective on the system.

And finally, thanks of course to Grace for her patience with me through this whole process.

Systematic Investigation of the Pr-Ba-Cu-O Phase Diagram

An Abstract of a Dissertation

Presented to

the Faculty of the Department of Physics

University of Houston

In Partial Fulfillment

of the Requirements for the Degree

Doctor of Philosophy

By

Lucas Galen Mastalli-Kelly

August 2019

ABSTRACT

This dissertation reports on an investigation into the longstanding mystery of why praseodymium barium cuprate is the only member of the $RBa_2Cu_3O_{7-y}$ family (which includes $RBa_2Cu_4O_8$ and $R_2Ba_4Cu_7O_{15}$) that has been synthesized with orthorhombic structure that is non-superconducting, juxtaposed with several contradictory reports of superconductivity. I walk through all of the possible contributors towards anomalous superconductivity based on existing reports: aluminum contamination/doping, alternate phases, and different stoichiometries. For all of these options, I find that the compounds are non-superconducting via magnetic and electronic measurements, only leaving the possibility of stress/strain induced superconductivity unexplored. In the process, I determine that the heat treatment reported to yield superconductivity in $PrBa_2Cu_3O_{7-\delta}$ (Pr123) results in the formation of significant quantities of $Pr_2Ba_1Cu_1O_5$ (Pr211) to form. I further establish that the three compounds: $PrBa_2Cu_3O_{7-\delta}$, $Pr_2Ba_4Cu_7O_{15-\delta}$ (Pr247), and $PrBa_2Cu_4O_8$ (Pr124), belong to a single incommensurate structure.

Contents

1	Background & Introduction	1
1.1	Introduction	1
1.2	Fundamental Properties of $PrBa_2Cu_3O_{7-\delta}$	2
1.2.1	A Note on Synthesis	4
1.2.2	Related Compounds	5
1.3	Reports of Superconductivity	10
1.3.1	Solid State Method Polycrystalline Samples	11
1.3.2	Traveling Solvent Floating Zone (TSFZ) Single Crystals	11
1.3.3	Self-Flux Single Crystals with Aluminum	13
1.3.4	Pechini Method Polycrystalline Samples	15
1.3.5	$Pr_2Ba_4Cu_7O_{15-\delta}$ Polycrystalline Samples	15
1.4	Doping Studies	17
1.4.1	Alkaline Earth (Ba) site	17
1.4.2	Rare Earth (Pr) site	18
1.4.3	Metal (Cu) site	19
1.5	Potential Explanations for Superconductivity	20
2	Methods	22
2.1	Sample Preparation	22
2.1.1	Pechini Method	22
2.1.2	Solid State Method	24

2.2	Thermal Measurements	24
2.2.1	TGA	25
2.2.2	DSC	25
2.3	Sample Characterization	26
2.3.1	XRD	26
2.3.2	Magnetic Susceptibility Measurements	26
2.3.3	Resistance	27
2.3.4	Heat Capacity	29
3	Experimental Results	31
3.1	Solid State Synthesis	32
3.1.1	Structure	32
3.1.2	Magnetism	32
3.2	Pechini Method	34
3.2.1	Structure	35
3.2.2	Magnetism	35
3.2.3	Heat Capacity	35
3.3	Pr_2BaCuO_5 (Pr211)	42
3.3.1	Magnetism	42
3.4	Al Doping	47
3.4.1	Structure/Purity	47
3.4.2	Magnetization	50
3.5	$Pr_2Ba_4Cu_7O_{15-\delta}$	53
3.5.1	Structure	53
3.5.2	Magnetism	53
4	Phase Diagram and Transitions	58
4.1	$PrBa_2Cu_3O_{7-\delta}$ in air	58
4.2	$Pr_2Ba_4Cu_7O_{15-\delta}$ in air	63
4.3	$Pr_2Ba_4Cu_7O_{15-\delta}$ in oxygen	64

4.4	$PrBa_2Cu_3O_{7-\delta}$ in reducing atmosphere	65
5	Conclusions	68

Chapter 1

Background & Introduction

1.1 Introduction

Despite intensive study over the past 30+ years, the nature of high temperature superconductivity remains elusive. There is no accepted, comprehensive theory which explains the presence of superconductivity beyond the temperature range permitted by BCS theory.

One of the longstanding mysteries is why only a single member of the $RBa_2Cu_3O_{7-y}$ family (which includes $RBa_2Cu_4O_8$ and $R_2Ba_4Cu_7O_{15}$) that has been synthesized with orthorhombic structure is non-superconducting. Of the rare earths, a total of four are not known to be superconducting in this structure [1]. The first is promethium, which is unstable and radioactive, preventing any serious attempts at synthesis. Next, neither cerium nor terbium appear in a trivalent state, preventing the synthesis of the orthorhombic structure. Praseodymium, however, forms compounds that are isostructural with the superconducting copper oxides [2].

Though the consensus view has long been that PBCO is non-superconducting, there are dissenters. To date, there have been reports of superconducting $PrBa_2Cu_3O_{7-\delta}$ (Pr123) in:

- powder [3]
- single crystal [4, 5], and

- polycrystalline forms [6].

Polycrystalline $Pr_2Ba_4Cu_7O_{15-\delta}$ has also been reported as superconducting by one group [7] with a lower T_c . The reported T_c for each form has been broadly consistent, and both doping and pressure measurements have indicated differences between the superconducting state in the praseodymium compound and the other rare earths, exemplified by yttrium. Unlike YBCO, PBCO shows continuing increase in T_c up to 10 GPa (the highest measured), with a far steeper slope [8]. This, along with the fact that the T_c of $Y_{1-x}Pr_xBa_2Cu_3O_y$ decreases with increasing x at least up to $x = 0.5$ indicate different superconducting states or mechanisms in the two materials [9].

1.2 Fundamental Properties of $PrBa_2Cu_3O_{7-\delta}$

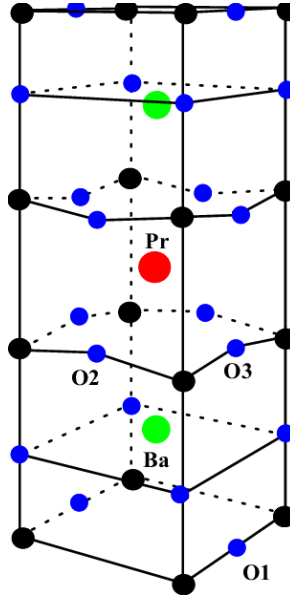


Figure 1.1: Pmmm structure of the $PrBa_2Cu_3O_{7-\delta}$ unit cell, with site designations [10].

The first real examination of the properties of $Y_{1-x}Pr_xBa_2Cu_3O_{7-y}$ was published in 1987, and lists Pr as having a stable tetravalent state [11], a claim I will address further. Diffraction measurements show the orthorhombic Pmmm structure of YBCO for all x , they note a convergence of the a - and b -axes with increasing x , indicating that the cell is tending towards a tetragonal cell [11]. However, it is well known that YBCO is superconducting

with both orthorhombic and tetragonal structures [12, 13, 14, 15], so the modern reader would find this unlikely to indicate a cause for any lack of superconductivity.

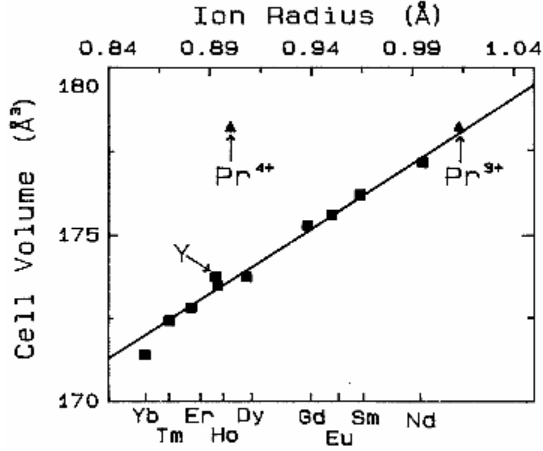


Figure 1.2: Cell volume vs ionic radii for $RBa_2Cu_3O_{7-\delta}$ with $R = Y$ and other rare earths except Ce and Tb. La, which has a larger ionic radius than even Pr^{3+} is also excluded [16].

When considering the effect of the rare earth ion size in the $RBa_2Cu_3O_{7-\delta}$ class, larger ionic radius leads to both slightly higher T_c and a compression of the Cu2-O4 distance due to chemical pressure. However, despite the large ionic radius, the doping with Pr reduced T_c at least through $x = 0.4$ [17]. Other than the predictable impact on cell volume due to a larger ionic radius, $PrBa_2Cu_3O_{7-\delta}$ is isostructural with the superconducting RBCO compounds.

Even as a non-superconductor, $PrBa_2Cu_3O_{7-\delta}$ is atypical. In materials that order with conventional antiferromagnetism (AFM), the Néel temperature is generally suppressed by increasing magnetic field. However no such change is seen up to 9 T [16]. Unlike YBCO where the non-superconducting magnetic properties are primarily attributed to the copper sites, PBCO's magnetic properties are dominated by Pr^{3+} 's moment.

One of the most frequently cited reasons for the destruction of superconductivity in the rare earth cuprates on the addition of Pr is that some of the Pr is tetravalent (as claimed by Solderholm *et al.* [11]) or mixed valence and thus reduces electronic hole concentrations in the copper oxide planes. One of the supporting arguments for this is the fact that for $PrBa_2Cu_3O_{7-\delta}$, $\mu_{eff} = 2.87\mu_B$ and the moment ionic praseodymium varies from $3.6\mu_B$

for Pr^{3+} to $2.5\mu_B$ for Pr^{4+} [18]. This would seem to indicate that the Pr site is of mixed valence; however, the moment is fully accounted for by crystal field effects and the 3+ valence alone [19, 20].

With the magnetization thus accounted for, most experiments support trivalent Pr, indicating instead that it may be strong hybridization of $\text{Pr}4f$ electrons and conduction holes in the Cu-O planes that quenches superconductivity by localizing mobile holes and inducing magnetic Abrikosov-Gorkov pair breaking [21, 22]. The hole localization and filling mechanism is supported by the fact that $\text{Pr}_{0.5}\text{Ca}_{0.5}\text{Ba}_2\text{Cu}_3\text{O}_{7-y}$ has been found to be superconducting with a $T_c \sim 40$ K in an epitaxial film- though it is unclear why this does not hold true for bulk samples [23].

1.2.1 A Note on Synthesis

It is very difficult to synthesize phase pure Pr123. Most groups report the presence of alternate phases, as determined by XRD, though not present for the superconducting single crystals. The primary alternate phase found is reportedly BaCuO_2 , which can be minimized by including an excess of $\sim 6\%$ Pr, though it is not eliminated entirely [18].

Importantly, many groups used relatively short calcination and sintering periods, for instance 15 hours in the case of Araujo-Moreira *et al.* [24]. However, some results suggest that 5-20 days are necessary to eliminate secondary phases [25].

Impurities aside, stoichiometric $\text{PrBa}_2\text{Cu}_3\text{O}_{7-\delta}$ is very nearly mythical, similar to other members of the RBCO class. This holds true independent of synthesis method. For the most samples presented in this study, a variation on the Pechini method was used for synthesis due to the increased homogeneity and decreased reliance on thorough mixing via mortar and pestle. Every sample measured was off stoichiometry. Though no single crystals were made for this study, others have found the same to be true of them. The differences do show some trends based on synthesis method, with flux grown crystals demonstrating a copper deficiency, for example [26].

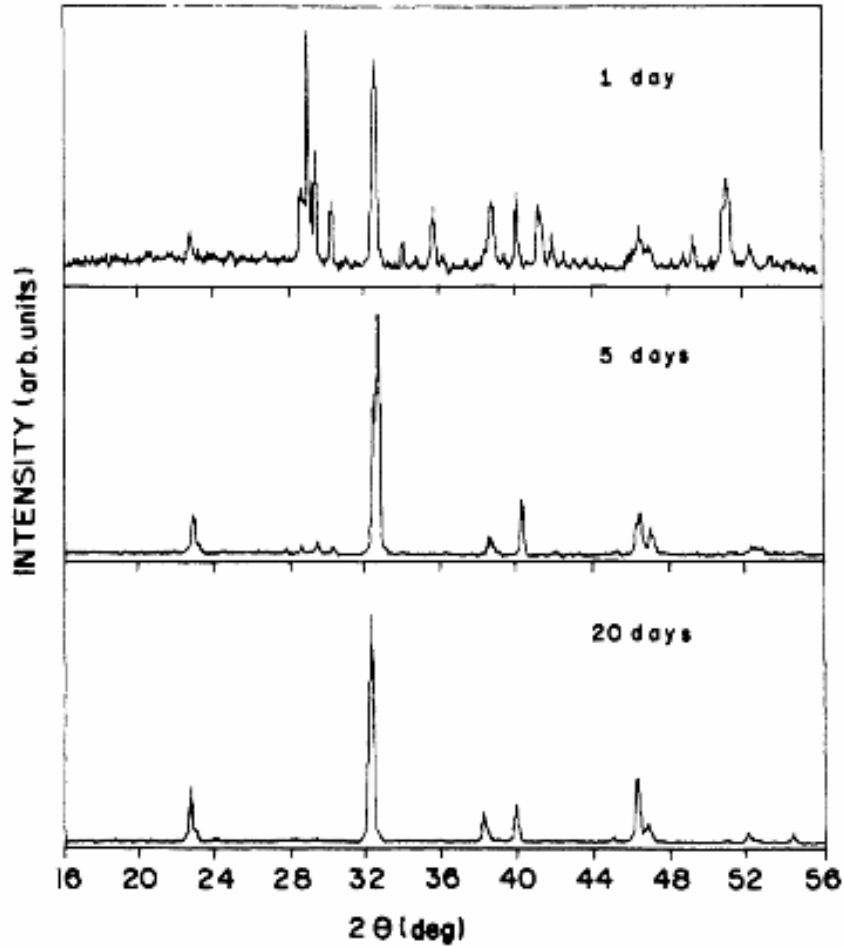


Figure 1.3: XRD pattern for three different annealing times. The one day used by many groups has significant impurity peaks. These shrink appreciably after five days, and all but vanish after 20. Solid state method, initial calcination at 900, later at 950. Quenched to room temp after final heating stage [25].

1.2.2 Related Compounds

There are a number of alternate phases which may appear during the synthesis of Pr123. Some of these are impurity phases caused by incomplete reaction of the constituents; ternary oxide compounds such as $BaCuO_{2+x}$ or $BaPrO_3$ are the most common such phases.

However, there are also alternate PBCO stoichiometries with similar structure and properties: Pr123 and Pr247. From XRD alone they are difficult to distinguish, as the best discriminator is a peak at $2\theta = 6.5^\circ$ for Pr124 (002), 7.0° for Pr247 (004), and 7.5° for Pr123 (001) [27]. For many XRD setups, including the one much of my data was collected

with, this cannot be made out against the low-angle background background.

Of particular interest in the discussion of superconductivity is the fact that in the $Y_{1-x}Pr_xBa_2Cu_3O_{7-\delta}$ system, the critical concentration of Pr to remove all superconductivity is $x_c = 0.5$. However for both the 124 and 247 analogues, it is $x_c = 0.8$ [27].

$PrBa_2Cu_4O_8$

The synthesis of $PrBa_2Cu_4O_8$ (Pr124) in an atmosphere of ambient pressure O_2 has been reported at a variety of temperatures from 850 – 885° C, with the phase determined via XRD [28, 29, 7, 30]. With the exception of Hagiwara *et al.* [7] differentiating the XRD pattern from that of Pr123 was not addressed. Hagiwara used the low angle peaks as described by Horii *et al.* and above. Lin *et al.* [30] used TGA as a differentiator, with the argument that their samples not losing mass until 800° C indicates that the samples are Pr124 as Pr123 is known to reduce at lower temperatures- however, their citation for this ([25]) has no TGA data and establishes no such thing, though my own data backs them up regarding Pr123.

Despite the lack of agreement on synthesis temperature, which Hagiwara *et al.* [7] viewed as very sensitive, there is some agreement on the properties. Unlike the single CO chained Pr123, Pr124 exhibits metallic conductivity at low temperatures, but shares antiferromagnetism with $T_N = 17$ K. No superconductivity has been reported in the system except for possibly in a mixed phase with $Pr_2Ba_4Cu_7O_{15-\delta}$, discussed below and in the following section.

$Pr_2Ba_4Cu_7O_{15-\delta}$

$Pr_2Ba_4Cu_7O_{15-\delta}$ (Pr247) has had reports of superconductivity in polycrystalline samples, and inconsistent reports of the non-superconducting properties. In particular, it is unclear whether or not there is an AFM transition, as both have been reported. The details of the superconducting results will be discussed in the next section.

An additional wrinkle is how difficult it can be to determine the purity of a sample. Pr123, 124 and 247 have nearly identical XRD spectra, with the primary differentiating

factor being the position of a low angle peak. Pr123 is positioned at 6.5, Pr124 at 7.5, with 247 in between at 7 even. On top of this, 247 is comprised of alternating blocks of 123 and 124, as seen in Figure 1.5. These factors combine to make it very difficult to discern from a mixed phase with anything less than atomic resolution, such as can be achieved with TEM.

Additionally, Pr247 is reportedly more difficult to synthesize than Pr123, due to a narrow temperature range of formation. Historically this has been obviated by using high oxygen pressure synthesis methods, but similar to Pr124 more recently- including the recent superconducting results- ambient pressure synthesis has been demonstrated.

Synthesis Methods

The method used by Hagiwara *et al.* [7] for their superconducting results is the citrate pyrolysis precursor method, which is similar the Pechini method used by Araujo-Moreira *et al.* [24] for Pr123 polycrystalline samples. The key differences are the higher temperature of formation for Pr247 885° C, and use of oxygen atmosphere. They also use a quartz tube and filter setup (Fig. 1.4) that I do not emulate.

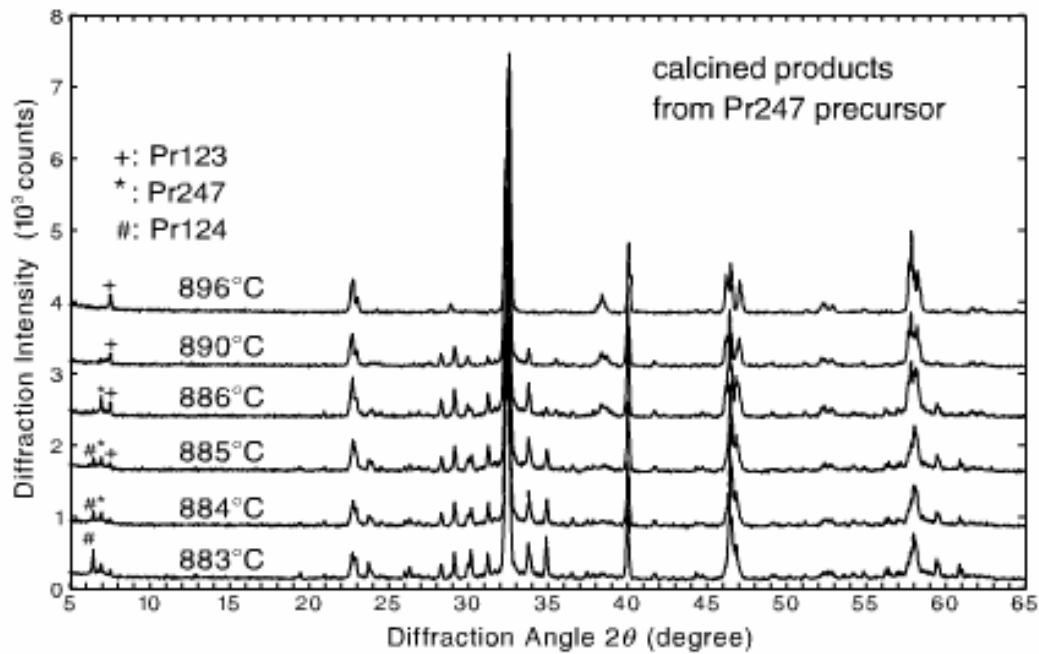
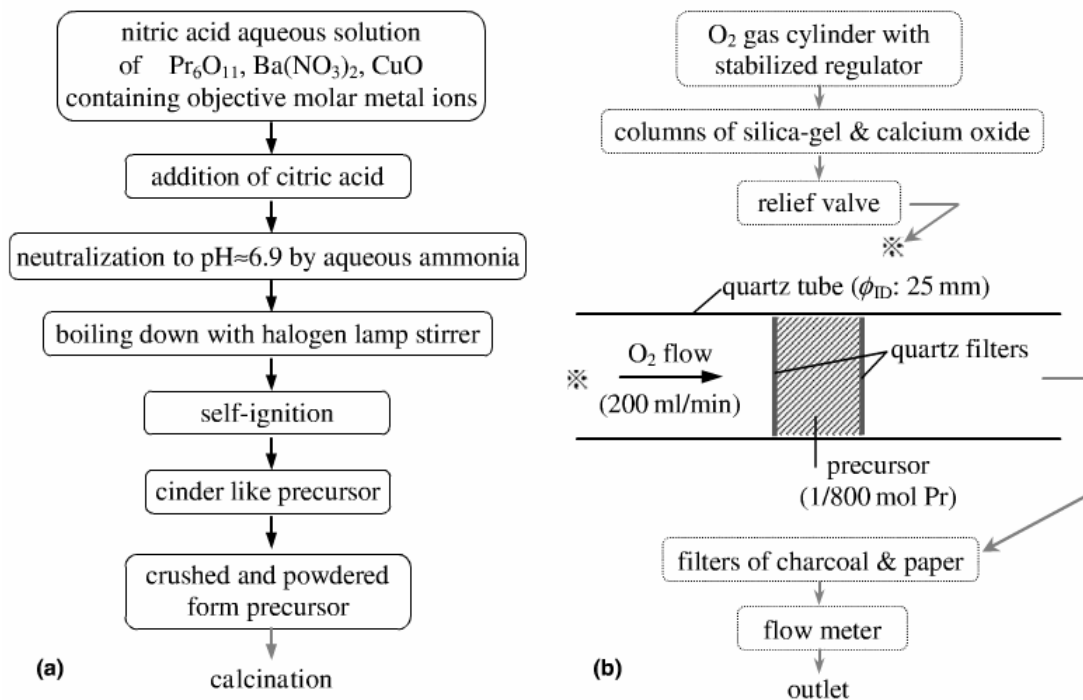


Figure 1.4: Even with this setup, high purity is difficult to achieve. Note in particular the high degree temperature sensitivity and lack of pure phase. Even for the best samples, 15-30 wt% Pr124 was present [7].

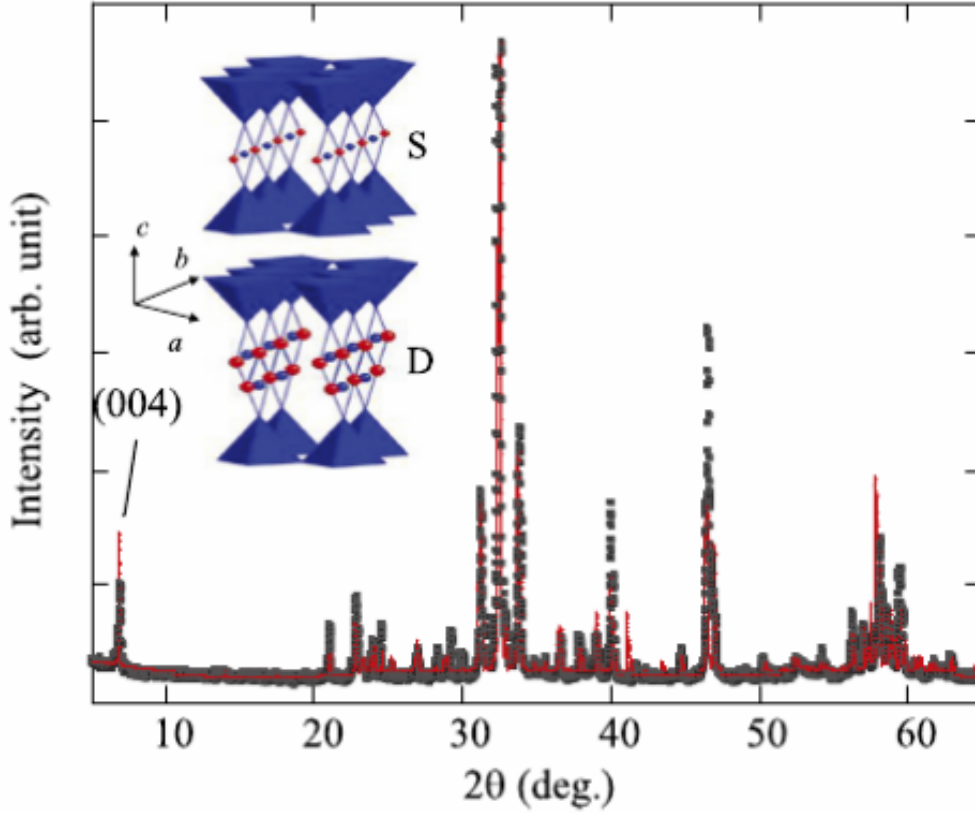


Figure 1.5: Measured XRD pattern for Pr247, with calculated pattern and structure inset [31].

Structure

The only way to confirm the structure of $Pr_2Ba_4Cu_7O_{15-\delta}$ is through use of transmission electron microscopy (TEM) measurements. Otherwise there is no way to ascertain where on the spectrum between single and double CO chains (Pr123 and Pr124) a sample lies. And it is truly a spectrum. The TEM measurements in Figure 1.6 show that prepared Pr247 samples do not always exhibit an alternating block structure of -D-S-D-S-, and can have longer period ordering such as -D-S-S-S-S-D-S-S-S-S- and samples are a heterogeneous combination of orderings [32].

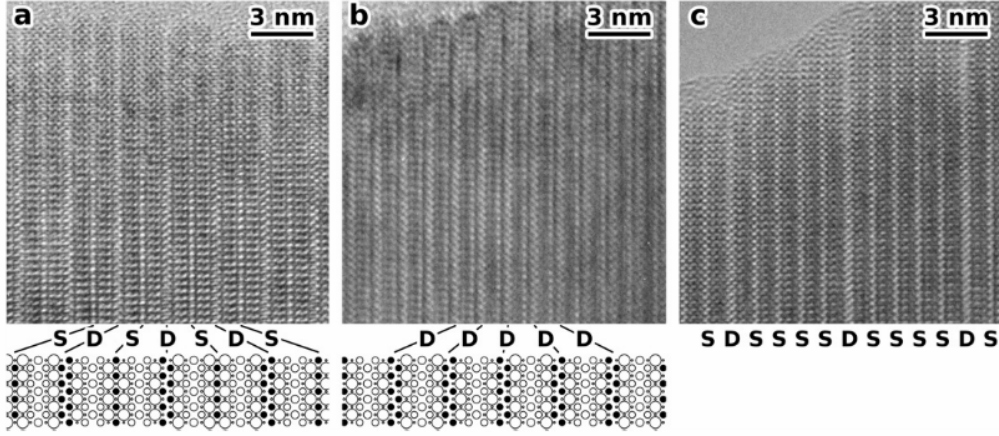


Figure 1.6: Three different areas of the same sample imaged with TEM. Different periodicity of the single and double Cu-O chains can be seen, denoted by S and D below each image. Structure is reported as Ammm, with $a = 3.8753 \text{ \AA}$, $b = 3.9107 \text{ \AA}$, $c = 50.713 \text{ \AA}$ [32].

1.3 Reports of Superconductivity

There are arguably three reasons for further study of the Pr containing RBCO compounds:

- Learning the reasons behind Pr's unique properties in the compounds (strong AFM, non-SC)
- Developing $PrBa_2Cu_3O_{7-\delta}$ as an insulating substrate for RBCO superconductors
- Investigating reports of superconductivity in $PrBa_2Cu_3O_{7-\delta}$ and $Pr_2Ba_4Cu_7O_{15-\delta}$

The third is all the more interesting for the number of independent groups to report it, with partial corroboration of each others specific results. Here I will review five sets of superconducting results, at a level of depth judged by the apparent credibility of the result. This list is not intended to be all inclusive, as I am aware of at least one additional group to have published a report of superconductivity, but it may be grouped with the less credible of the polycrystalline results discussed below. The first several results discussed are all concerning $PrBa_2Cu_3O_{7-\delta}$ while the last regards $Pr_2Ba_4Cu_7O_{15-\delta}$.

1.3.1 Solid State Method Polycrystalline Samples

The first report of superconductivity in the system known to me comes from Drs. Howard A. Blackstead and John D. Dow, who have published a number of papers together and separately regarding both experimental results and (primarily on the part of Dow) theoretical explanations. In their first report, they claim to find a 7% superconducting volume percentage on the basis of resistance data in thin films, and a drop in the number of unscreened spins in an ESR signal, showing transitions at 92 K [3]. The thin film results were reproduced using a YBCO substrate by Usagawa *et al.* the following year [33]. However, they are unable to reliably produce superconducting samples, despite many attempts under different conditions, and are unable to observe the Meissner effect via conventional measurements without subtracting a large ‘paramagnetic background’ [34]. Best results are seen in low oxygen environments when there is partial melting, which I will show in the following chapters means impurity phases and contamination are likely. Their operating theory is that it is Pr on the Ba sites which suppresses superconductivity, and thus they are only able to see superconductivity in small regions with below a critical density of that particular defect. While they do show that such defects exist, the thesis is not proven [35].

Their results could most easily be explained by a diamagnetic transition in an impurity phase such as $BaCuO_{2+x}$ as has sometimes been reported at high temperatures [36].

1.3.2 Traveling Solvent Floating Zone (TSFZ) Single Crystals

Zou *et al.* [37] have some of the most thoroughly reported superconducting results for Pr123, with magnetization, resistance, and pressure measurements. Importantly, they are the only authors who report bulk superconductivity in Pr123 based on their measurements of the Meissner effect and zero resistance [4]. However, that estimate of volume fraction takes into account a ‘demagnetization factor’ which is not proven to be intrinsic to the sample. The field cooled data shows the Meissner effect in 15% of the total volume. Given both this and the sizeable ΔT_c , I would argue that the superconductivity is in well under 100% of the crystal. Similar to the above polycrystalline samples, the TSFZ synthesis was conducted

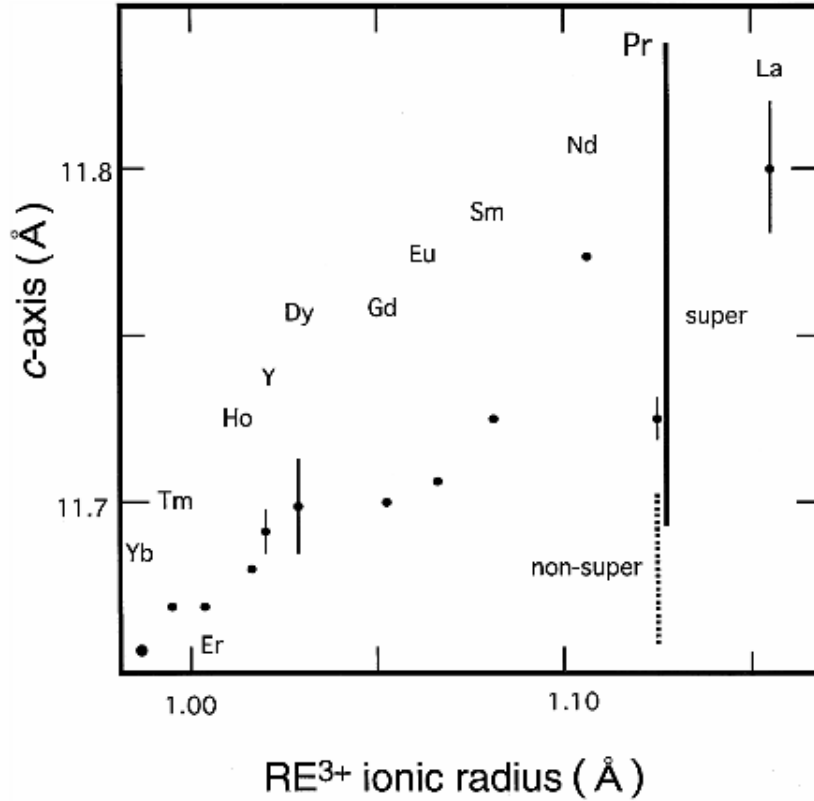


Figure 1.7: RE^{3+} -ionic-radius dependence of the c -axis length in R123 system. The solid line is the range measured for superconducting single crystals, and the dotted line that of non-superconducting crystals [38].

in a low oxygen environment. A thorough study and comparison of superconducting and non-superconducting crystals was conducted, as both were present within the same TSFZ rod, showing a longer c -axis on average for the superconducting samples [38].

Detailed conditions for TSFZ synthesis are reported, but no publications by other groups replicating superconductivity with them could be found, though the next set of results discussed attempts to imitate some of the conditions without the TSFZ procedure.

This set of single crystal results also contains the first real experimental evidence that the character of the superconductivity in this system may differ from that of other RBCO compounds. Pressure measurements show a far steeper increase in T_c than is seen for the other compounds [37, 8]. This is evidence in support of Blackstead and Dow's assertion that superconductivity in the compound exists in the Ba-O planes [39]. However, Dow later

makes the same claim for YBCO, casting some doubt on the veracity of such a claim [40]. Nevertheless, many other theorists have put forward models for superconductivity in the system existing outside of the copper oxide planes in this system, contrasting with YBCO [41, 42, 43].

It is difficult to evaluate the exact synthesis conditions given that heat is provided via infrared lamps and not measured directly, but this set of results is robust and likely measures superconductivity. Whether or not that superconductivity occurs within Pr123 or some other phase is less certain. For instance, one response to the results argues that a thorough review of the magnetization data suggests about 50% substitution of Ba at the Pr sites in the superconducting crystals [44].

1.3.3 Self-Flux Single Crystals with Aluminum

Luszczek *et al.* deliberately tried to replicate the above results by making self-flux single crystals with a high temperature reduction followed by a lower temperature oxygen anneal. Their most interesting finding was that they only found superconductivity for crystals synthesized in alumina crucibles (Figure 1.1), with up to 30% substitution of aluminum for copper in the Cu-O chains [5].

The influence of aluminum and other dopants on the copper sites will be discussed in more depth in the next section. However, it is worth noting that there is some logic to the notion that aluminum might have a larger impact on $PrBa_2Cu_3O_{7-\delta}$ than YBCO, where it only slightly degrades the T_c as it can be seen in Figure 1.2 that it has far higher integration into Pr containing single crystals [45]. Also of interest is the fact that this superconductivity reportedly fades over the course of about two weeks [46]. This combined with the high temperature and quick quenching in reducing atmosphere required to achieve superconductivity suggests that an internal stress/strain effect within their single crystals may be the key factor, possibly due to the formation of an impurity phase.

Sample number	$T_{red}/t_{red}/v$ ($^{\circ}\text{C}/\text{h}/\text{Q}$ or S)	$T_{ox}/t_{ox}/v$ ($^{\circ}\text{C}/\text{h}/\text{Q}$ or S)	T_c (K)	Crucible
1 (A)	–	460/96/S	–	Al_2O_3
2	800/10/S	460/72/S	–	ZrO_2
3	900/10/S	460/48/S	–	Al_2O_3
4	900/5/S	350/48/S	–	Al_2O_3
5	900/5/Q	350/48/S	–	ZrO_2
6	950/3/Q	460/48/S	–	ZrO_2
7	950/3/Q	350/48/S	–	Al_2O_3
8	970/3/Q	350/72/S	30	Al_2O_3
9	970/3/Q	460/72/S	26	Al_2O_3
10 (B)	980/2/Q	460/72/S	56	Al_2O_3
11	980/2/Q	460/72/S	–	ZrO_2
12 (C)	980/2/Q	350/72/Q	82	Al_2O_3
13	980/2/Q	350/72/Q	–	ZrO_2
14	990/2/Q	350/72/S	88	Al_2O_3
15	990/2/Q	350/72/S	–	ZrO_2
16	990/2/S	350/72/S	–	ZrO_2
17	1000/2/Q	360/72/S	62	Al_2O_3
18	1000/2/S	360/72/S	–	Al_2O_3

Table 1.1: The thermal treatments given self flux grown crystals after growth by Łuszczek *et al.*, with resulting superconducting properties if present as determined by ac susceptibility measurements. Notations: $T_{red,ox}$; $t_{red,ox}$; temperature and time, respectively, of the reduction and oxidation process; v: cooling rate (Q, S: quick and slow). Of particular note is the presence of superconductivity only in crystals reduced at temperatures of 970° C or higher, quenched quickly, and synthesized in alumina crucibles [5].

Nominal composition	Measured composition (EDX)	Percentage of Al in the $\text{Cu}_{1-x}\text{Al}_x\text{O}_{1-\delta}$ chains	
		(EDX)	(Raman)
$\text{Y}_1\text{Ba}_2\text{Cu}_3\text{O}_{7-\delta}$	$\text{Y}_{0.99}\text{Ba}_{2.01}\text{Cu}_{2.92}\text{Al}_{0.08}\text{O}_{7-\delta}$	8	10
$\text{Y}_{0.9}\text{Pr}_{0.1}\text{Ba}_2\text{Cu}_3\text{O}_{7-\delta}$	$\text{Y}_{0.87}\text{Pr}_{0.14}\text{Ba}_{1.99}\text{Cu}_{2.88}\text{Al}_{0.12}\text{O}_{7-\delta}$	12	14
$\text{Y}_{0.8}\text{Pr}_{0.2}\text{Ba}_2\text{Cu}_3\text{O}_{7-\delta}$	$\text{Y}_{0.73}\text{Pr}_{0.26}\text{Ba}_{2.05}\text{Cu}_{2.80}\text{Al}_{0.16}\text{O}_{7-\delta}$	16	13
$\text{Y}_{0.7}\text{Pr}_{0.3}\text{Ba}_2\text{Cu}_3\text{O}_{7-\delta}$	$\text{Y}_{0.68}\text{Pr}_{0.37}\text{Ba}_{1.95}\text{Cu}_{2.83}\text{Al}_{0.17}\text{O}_{7-\delta}$	18	16
$\text{Y}_{0.6}\text{Pr}_{0.4}\text{Ba}_2\text{Cu}_3\text{O}_{7-\delta}$	$\text{Y}_{0.56}\text{Pr}_{0.47}\text{Ba}_{1.97}\text{Cu}_{2.69}\text{Al}_{0.31}\text{O}_{7-\delta}$	31	24
$\text{Y}_{0.5}\text{Pr}_{0.5}\text{Ba}_2\text{Cu}_3\text{O}_{7-\delta}$	$\text{Y}_{0.53}\text{Pr}_{0.46}\text{Ba}_{2.02}\text{Cu}_{2.70}\text{Al}_{0.29}\text{O}_{7-\delta}$	29	20
$\text{Y}_{0.4}\text{Pr}_{0.6}\text{Ba}_2\text{Cu}_3\text{O}_{7-\delta}$	$\text{Y}_{0.39}\text{Pr}_{0.59}\text{Ba}_{2.06}\text{Cu}_{2.81}\text{Al}_{0.15}\text{O}_{7-\delta}$	31	23
$\text{Y}_{0.2}\text{Pr}_{0.8}\text{Ba}_2\text{Cu}_3\text{O}_{7-\delta}$	$\text{Y}_{0.21}\text{Pr}_{0.80}\text{Ba}_{2.00}\text{Cu}_{2.71}\text{Al}_{0.28}\text{O}_{7-\delta}$	28	24
$\text{Pr}_1\text{Ba}_2\text{Cu}_3\text{O}_{7-\delta}$	$\text{Pr}_{0.99}\text{Ba}_{2.04}\text{Cu}_{2.68}\text{Al}_{0.29}\text{O}_{7-\delta}$	29	23

Table 1.2: The amount of aluminum found to have replaced copper in a variety of $\text{Y}_{1-x}\text{Pr}_x\text{Ba}_2\text{Cu}_3\text{O}_{7-\delta}$ single crystals with different Pr content, as measured by both EDX and Raman spectroscopy. According to the Raman results, all of the aluminum goes to the Cu-O chains rather than the copper oxide planes [45].

1.3.4 Pechini Method Polycrystalline Samples

There have been a couple of workers to publish superconducting results for samples made via the Pechini method [24, 7], including some details of the technique used. The idea here is that Pr on Ba site disorder leads to pair breaking inhibiting superconductivity, and that the improved homogeneity and structure of a sol-gel method where citric acid (a chelating agent) coordinates the metal ions prior to calcination will thus lead to higher quality polycrystalline samples [6]. While there is no evidence that this method has any impact on Pr on Ba site disorder, both my results and others can support the increased homogeneity granted by this methodology.

Unfortunately, this set of results is well in line with those published by Blackstead and Dow. They see a very low superconducting volume fraction, and only when subtracting out a significant paramagnetic background to see a very small diamagnetic signal. They share no resistance measurements, and the heat capacity data they share is inconclusive [24]. It is very likely that any effect seen here is an impurity phase, not necessarily superconducting, present in a very small amount of the sample.

1.3.5 $Pr_2Ba_4Cu_7O_{15-\delta}$ Polycrystalline Samples

Lastly, I consider the reports of superconductivity not in $PrBa_2Cu_3O_{7-\delta}$ (Pr123) but $Pr_2Ba_4Cu_7O_{15-\delta}$ (Pr247), which was synthesized via a ‘citrate pyrolysis’ method very similar to the Pechini method above, conducted in 1 atm oxygen [7]. Hagiwara *et al.* publish thorough magnetic, resistance and heat capacity measurements, the first two of which point towards superconductivity in up to 35% of the bulk, though with a large ΔT_c indicating what may be filamentary superconductivity at 26.5 K. Their synthesis conditions and structural results are discussed in the prior section. In particular, TEM indicates that their samples are not periodic Pr247, but an incommensurate crystal structure where the alternation of single and double Cu-O chains is only periodic over short distances. They suggest that it may be the regions which are rich in double Cu-O chains, or $PrBa_2Cu_4O_8$ (Pr124) that contain superconductivity.

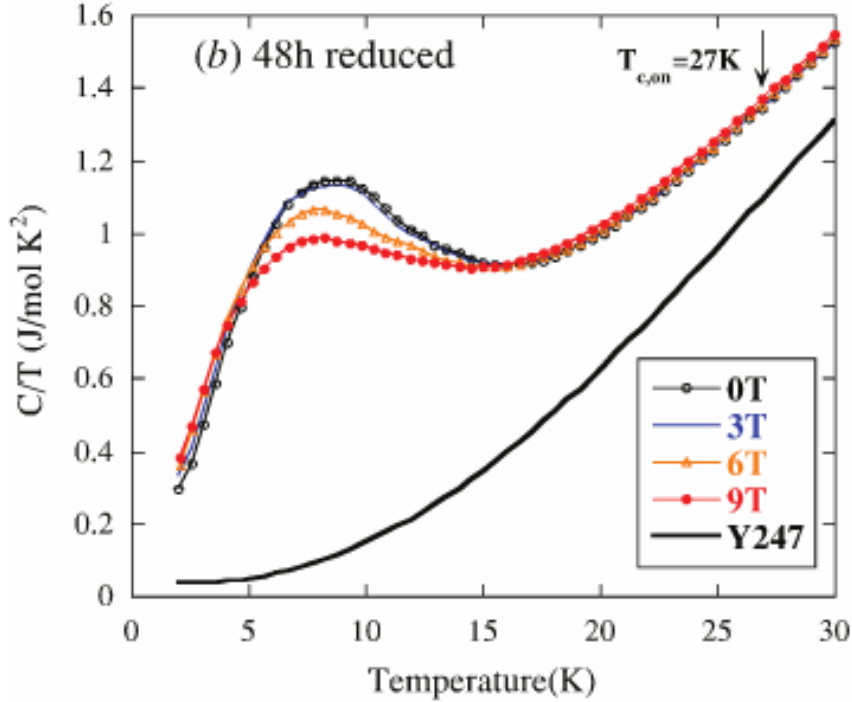


Figure 1.8: Heat capacity for a reduced nominal Pr247 sample. The authors claim that a Schottky type specific heat maximum obscures the superconducting transition (see reference for fit), but a more logical explanation is a broadened AFM lambda transition and no superconducting transition [47].

On top of this, the heat capacity data of their reduced samples does not show a superconducting transition. The authors claim that it is obscured by a Schottky type specific heat maximum, and provide a fit with parameters that approximately fit the peak seen in Figure 1.8 [47]. However, to a critical eye, this simply appears to be the same antiferromagnetic (AFM) lambda transition that is present in their as-sintered sample, broadened and moved to a lower temperature as expected to occur with the Néel temp as the oxygen content is heterogeneously lowered in Pr123. Even if there is a very small electronic contribution to the specific heat, there should be visible splitting at high field at the transition, which is not seen in their results, nor does their fit do anything to obscure the higher temperature region where their T_c is reported [48].

Despite the questions raised by their heat capacity data, these are the only high quality superconducting results for the PBCO family in polycrystalline samples, as well as for

Pr247. Despite the relatively low transition temperature, it is possible that double Cu-O chains of the phases identified here are also forming in the nominal Pr123 samples reported above and carry responsibility for the superconductivity. Or, there could be two different superconducting mechanisms within the PBCO system. Of course, given that none of the results reported here has been independently repeated, and none of them have been able to produce a full set of measurements firmly demonstrating superconductivity beyond a reasonable doubt, it is possible that impurities, contamination and error explain all of the results reported above. By following some of their procedures, it may be possible to determine the origin of their results. I also consider the possible influence of a variety of contaminants or dopants, which may also give hints as to mechanism behind the general lack of superconductivity in the system.

1.4 Doping Studies

1.4.1 Alkaline Earth (Ba) site

It is well known that Pr123 frequently has some fraction of Pr and Ba swap sites due to their similarity in size. Calcium in particular is likely to appear at the rare earth site [49]. So while $PrBa_{2-x}Ca_xCu_3O_{7-y}$ has been nominally synthesized, there is no confirmation that it is not in reality $(Pr_{1-x}Ca_x)(Ba_{2-x}Pr_x)Cu_3O_{7-\delta}$, or some combination of the two. [50] Ba site Pr is also one proposed explanation for the suppression of superconductivity in the system [51, 46].

This makes strontium (Sr) the best, and perhaps only reliable, alkaline earth dopant, with a bulk solubility in $PrBa_{2-x}Sr_xCu_3O_{7-\delta}$ of $x = 0.8$, with a steady decrease in the resistivity with increased doping and an orthorhombic to tetragonal transition at $x = 0.2$ [52]. No change in the magnetic moment of Pr is seen for bulk samples. The amount of Sr included in the structure can be increased through the use of non-equilibrium synthesis methods, such as pulsed laser deposition. This, performed on an LAO substrate shows that resistivity continues to decrease through an insulator to metal transition somewhere $x > 1.6$, with $x = 2.0$ being metallic down to 60 K, where it resumes semiconductor-like behavior,

though the reason for this reversal is unclear [53, 54, 55]. No magnetic measurements were reported for the thin films in these studies.

However, $Y_{0.4}Pr_{0.6}Ba_{2-x}Sr_xCu_3O_7$ has also been studied. In this case, increasing Sr concentration is also seen to increase carrier concentration, restoring metallic conduction and even going one step further to induce superconductivity for $x = 0.8, 1.0$ [56]. However, as the addition of Sr shortens the c -axis, this is likely superconductivity of the same character as YBCO and unlike what is seen in the traveling solvent floating zone (TSFZ) results.

1.4.2 Rare Earth (Pr) site

As mentioned above, both $PrBa_{2-x}Ca_xCu_3O_{7-y}$ and $(Pr_{1-x}Ca_x)Ba_2Cu_3O_{7-\delta}$ have nominally been studied. In both cases, T_N is suppressed, though Ba site doping has a stronger effect, believed to be due to atomic disorder whereas the Pr site effect is dilution. Resistivity lowers in both cases, but similarly sees more change when Ca is nominally on the Ba site [50].

The bulk solubility of Ca in Pr123 is $x \leq 0.3$ for the Pr site. However, one of the most interesting results in the compound occurs for $0.4 \leq x \leq 0.5$ where metastable thin films exhibit superconductivity with an onset T_c as high as 47 K, and $T_c(R = 0)$ of 35 K.[23] Notably, this is higher than the T_c seen for doping with the same amount of yttrium for either thin films or many bulk samples [57, 11]. The a - and b -axes decrease with Ca content, while the c -axis increases.

When doped with other rare earths (that do form superconducting compounds), the results are generally similar, though the critical concentration of Pr needed to suppress superconductivity varies; it is lower for Gd than Y, for example [21].

Barium doping has also been done on the rare earth site. Barium on the rare earth site and Pr on the alkaline earth site have, in a number of variations, been credited with both the suppression of superconductivity and in the compound and its rare occurrence [44, 58]. When doped on the Pr site, Ba increases the carrier (hole) concentration though it is unclear what band the additional carriers are in. This leads to a decrease in the resistivity. Carrier concentration is maximized at $x = 0.2$, with no change at $x = 0.3$, potentially indicating

the solubility limit [59].

1.4.3 Metal (Cu) site

Doping of the metal site has attracted relatively little interest when it comes to determining why YBCO-like superconductivity does not occur in the praseodymium system. This is due to the role of the copper oxygen planes in housing the superconducting carriers in the R123 system. In YBCO, most substitutions for copper are damaging to superconductivity. Fe and Al substitution maintain T_c up to 5 and 10% respectively, whereas by 10% Ga substitution superconductivity is eliminated entirely. Up to 5% Co substitution leads to modest increases in T_c . Similarly, Mo substitution to nearly 10% enhances J_c and T_c [60]. Mo can also be used to stabilize structures with higher doping levels, allowing other dopants to be used try to add additional carriers to the Cu-O layers [61]. In $Y_{1-x}Pr_xSr_2Cu_{2.7}Mo_{0.3}O_{7-y}$, it is used to allow full substitution of Sr for Ba. In this compound, the critical concentration of Pr to completely suppress superconductivity is about 0.85, far in excess of the 0.5 – 0.65 range required in $Y_{1-x}Pr_xBa_2Cu_3O_{7-y}$ [62]. This is particularly curious given that the T_c at $x = 0$ is only 33.2 K.

Zn doping to 10% (0.3) alters the magnetic structure- introducing ferromagnetic order along the c -axis while antiferromagnetic order is maintained in the a - b plane, along with a T_N of 17 K [63]. However, it is not clear if all of the Zn in fact fully dissolved into the structure. There is some doubt, given that in YBCO the solubility is only up to 0.22. When incorporated into YBCO, it both suppresses the superconductivity and increases the suppression by Pr doping. The cause of the suppression is unclear, as unlike Pr it is less than the impact predicted by Abrikosov-Gor'kov theory [64].

Of some note, is that Zn and Ni are both believed to substitute into the CuO_2 planes, whereas most other dopants (including Ga and Al) go to the CuO chains. This may be the reason Zn does not impact the macroscopic magnetic properties, but *Ga* doping lowers T_N [22, 65].

The most common doping at the Cu site is Al, for the simple reason that it is mostly accidental and alumina crucibles are among the most common. This is especially true for single

crystals. As with Ga, Al lowers T_N and appears in the CuO chains according to Raman data [66, 45, 67]. It is unclear if the contamination also occurs in polycrystalline samples, but it seems likely given that many groups report performing calcination between 900° C and 950° C, where PBCO melts incongruently when in Argon or low oxygen atmosphere.

1.5 Potential Explanations for Superconductivity

A response published to Zou et al’s single crystal results notes that the μ_{eff} reported above the T_c is inconsistent with the $\chi(t)$ shown for their superconducting single crystals, but that both this inconsistency and the reported difference in c-axis length could be explained by Ba substituting at about half of Pr sites in the superconducting crystals [44]. This is feasible given the nature of traveling solvent floating zone (TSFZ) synthesis and that only some crystals from the boule were superconducting.

This also makes sense in the context of the superconducting, Ca doped, thin film. However, when $Pr_{1-x}Ca_xBa_2Cu_3O_{7-y}$ is synthesized in bulk, the solubility limit appears to be around $x = 0.3$ [68].

Considering the fact that the most reliable superconducting results for $PrBa_2Cu_3O_{7-\delta}$ are from single crystals, it is possible intrinsic stress/strain is a factor. This would also help explain difficulties in reproduction, and the disappearance of superconductivity in the crystals over time after annealing [5].

There are at least two other possible factors: accidental aluminum doping from alumina crucibles and the presence of other Pr-Ba-Cu-O compounds, such as Pr247. Even neglecting ternary impurities, the high temperature anneal performed by Luszczek et al. is in a temperature range where melting and the formation of Pr_2BaCuO_5 can occur; $PrBa_2Cu_3O_{7-\delta}$ melts at 971° C in air, and lower temperatures at low oxygen pressures. Furthermore, the same group only saw superconductivity in crystals prepared using alumina crucibles [5].

To avoid the complexities of single crystal synthesis, and given that the only effect that might cause superconductivity in them and not polycrystalline samples is difficult to replicate stress/strain, my study will focus on the influence of aluminum and alternate

phases. As there is some speculation regarding even the basic materials properties at times, and how they are influenced by different synthesis methods, I will also be investigating several of the techniques previously reported to yield superconductivity in an attempt to reproduce or refute those results.

Chapter 2

Methods

2.1 Sample Preparation

I personally prepared and synthesized all samples used for this research. Polycrystalline samples were prepared primarily via the Pechini (citric acid sol-gel) synthesis method [69]. A few samples were prepared via the standard solid state route for comparison, but were generally less homogeneous.

For most samples, alumina crucibles were used. As will be discussed later it is known that aluminum can leach from crucibles to replace copper in the cuprates, and this happens at a much higher rate for compounds with praseodymium than yttrium [45]. Thus for some samples, I used specially prepared alumina crucibles prepared coated with $BaZrO_3$. This has been shown to be non-reactive with the cuprates.[67, 70] The preparation procedure is based on that of [70], and is part of an ongoing collaboration with Dr. James Meen and his student Tanvi Parikh.

2.1.1 Pechini Method

Materials:

- $BaCO_3$
- aqueous citric acid solution or citric acid

- CuO
- HNO_3
- $Pr(NO_3)_3 \cdot 6H_2O$
- Ethylene glycol
- Ethylene diamine
- mortar + pestle
- micro pipettes
- two Pyrex beakers

Use molar quantities of all precursors for the intended composition, or in the ratio indicated below for chelating and gelling agents. All quantities given below are for 0.5g of Pr123 sample.

Procedure:

1. Use a pyrex beaker for sol-gel preparation
2. Dissolve 0.275g $BaCO_3$ in aqueous citric acid solution. (1.205g citric acid, 6.27×10^{-3} mol) (3:1 citric acid metal/copper mole ratio)
3. Dissolve 0.166g CuO in HNO_3 and add to mixture. Start with 10 mL of acid, dilute with DI water.
4. Add $Pr(NO_3)_3 \cdot 6H_2O$ (0.3028g is molar quantity)
5. Add 1.807g (1.624 mL) ethylene glycol (citric acid:ethylene glycol mass ratio of 60:40)
6. Resulting solution should be blue
7. Neutralize solution with ethylene diamine (0.8 mL of ethylene diamine per mL of nitric acid to neutralize). Goes to deep blue.
8. Check pH. Add ethylene diamine or nitric acid as needed to neutralize.

9. Place on hot plate on low/medium low (setting 3/10) until reduced down to a gel, or to the point where the gel expands into an ash structure.
10. Heat at 400° C for 12 hours in the Pyrex container to burn off all volatile compounds in air.

From this point the precursor may be used just as the precursors in the solid state method are. They should first be reacted at high temperature to remove any remaining nitrates or carbonates, then pressed into pellets for calcination [69].

2.1.2 Solid State Method

Stoichiometric quantities of Pr_6O_{11} , CuO and $BaCO_3$ powder were combined and ground thoroughly with an agate mortar and pestle. This was first reacted at 850° C for at least 24 hr, then re-ground and pressed into pellets. These pellets were then calcined and annealed in tube furnaces following the same procedures as with the Pechini method.

2.2 Thermal Measurements

In order to determine the phase diagram of the Pr-Ba-Cu-O system, a number of thermal measurements were completed up to high temperatures to determine where phase transformations occur. For these measurements, a Netzsch Simultaneous Thermal Analyzer - STA 449 F1 Jupiter was used for TGA and DSC measurements in the TAPAF user facility within TCSUH. The silicon carbide furnace was utilized along with alumina crucibles. The STA is vacuum-tight to 10^4 mbar, giving high confidence that the desired atmosphere is experienced by the samples [71].

For these measurements, powder was provided to the equipment operator, Tatyana Makarenko, who pressed an appropriate amount into a pellet and conducted the measurements.

2.2.1 TGA

Thermo-gravimetric analysis (TGA) uses a sensitive balance to measure changes in the mass of a sample as it is heated and cooled. This can be used to determine when certain compounds burn off- such as carbonates forming carbon dioxide- or the loss or uptake of oxygen (or other gasses) from the system. As all samples measured for this study are expected to be fully reacted with no remaining carbonates or similar, it is expected that all gains and losses measured via TGA are due to oxygen. TGA can also reveal the nature of some reactions- if there is a change in slope of the TGA curve at the same temperature as a peak in DSC or DTA measurements, it can indicate the change in oxygen stoichiometry of the reaction. If there is none, it indicates that the oxygen content remains constant during that reaction.

For the STA 449 F1 Jupiter, the balance has a resolution of 25 ng, and a balance drift of less than 2 μg per hour. For samples on the order of 20 mg, such as those used here, this results in an effective drift of under 0.1% per hour, much lower than the rate of change seen in my own measurements and thus of no impact on results.

2.2.2 DSC

Differential Scanning Calorimetry (DSC) measures the heat needed to increase the temperature of a sample relative to a standard reference while temperature is changed. This allows measurement of changes in the heat capacity and clearly indicates transitions that either absorb or release heat, such as phase transitions, structural transitions, and exo or endo thermic chemical reactions.

The STA 449 F1 Jupiter has an accuracy of $\pm 2\%$ measuring the enthalpy of most samples, and allows for heating rates from 0.01-50 K/min. Due to the melting of $\text{PrBa}_2\text{Cu}_3\text{O}_7$ at 971°C , for most measurements I used a maximum temperature of 950°C for measurements in air. The melting temperatures in other atmospheres have not been established.

2.3 Sample Characterization

2.3.1 XRD

X-Ray Diffraction (XRD) measurements were used to determine the structure of all samples. All XRD data shared here was taken with the Rigaku Smart Lab system in the TCSUH user lab.

The principle behind XRD is that measuring the diffraction pattern of radiation with a known wavelength and source position can reveal the crystalline structure of a powder or single crystal sample. The crystal or polycrystalline sample behaves as a diffraction lattice, causing scattering in accordance with Bragg's law of diffraction, where d is the lattice spacing and n is an integer.

$$n\lambda = 2d \sin \theta$$

2.3.2 Magnetic Susceptibility Measurements

Measurements of sample magnetic susceptibility were conducted with Quantum Design's line of SQUID magnetometers, notably the Magnetic Properties Measurement System (MPMS) and MPMS 3. The two systems have different designs and temperature control systems, but are based on the same core principle of moving a sample within magnetic coils to measure the response.

Measurements of the magnetization with change in temperature (MT) were conducted on the MPMS between 2 K and 300 K. I determined that the remnant field, even after degaussing, can be on the order of 10 Oe, thus most measurements shared here were done with a minimum of 50 Oe, and the molar susceptibility is calculated from measurements performed at 1 kOe or greater. Magnetization measurements with change in field (MH) utilized the MPMS 3.

2.3.3 Resistance

All resistance measurements were carried out on an in-house built dip probe and electronic systems. The electronic systems consisted of a Lakeshore 336S temperature controller, Keithley 2400 source meter, and Keithley 6517A high resistance meter. The LR700 (Linear Research) alternating current resistance bridge was used for some initial measurements.

For measurements of superconductors, metals, and other relatively low resistance materials at low temperature, a four lead measurement is traditionally used. This is due to the fact that with a low sample resistance, contact and lead resistance will dominate in a two lead measurement (Fig 2.1).

$$V_{meas} = (I - \varepsilon)(2R_{lead} + 2R_{contact} + R_{sample}) - 2\varepsilon r_{lead} \quad (2.1)$$

However, in the four lead configuration, the lead and contact resistances have a much lower impact on the measured voltage.

$$V_{meas} = (I - \varepsilon)R_{sample} - 2\varepsilon(r_{lead} + r_{contact}) \quad (2.2)$$

However, in my measurements, it was found that samples often had very high resistances. In some cases, they even behaved as dielectrics, exhibiting capacitor behavior. Such a high resistance, many orders of magnitude above the contact and lead resistances, removes the advantages of the four lead measurement. Furthermore, given that the current ε grows in proportion with the sample resistance, it can become non-negligible should the sample resistance approaches the internal resistance of the voltmeter.

$$\frac{\varepsilon}{I - \varepsilon} = \frac{R_{sample}}{R_{internal} + 2r_{contact} + 2r_{lead}} \quad (2.3)$$

All samples measured exceeded the maximum resistance measurable with the experimental setups available to me at low temperature. Many samples exhibited surface resistances at room temperature in or near the mega-ohm range. As such, few resistance measurements are reported herein.

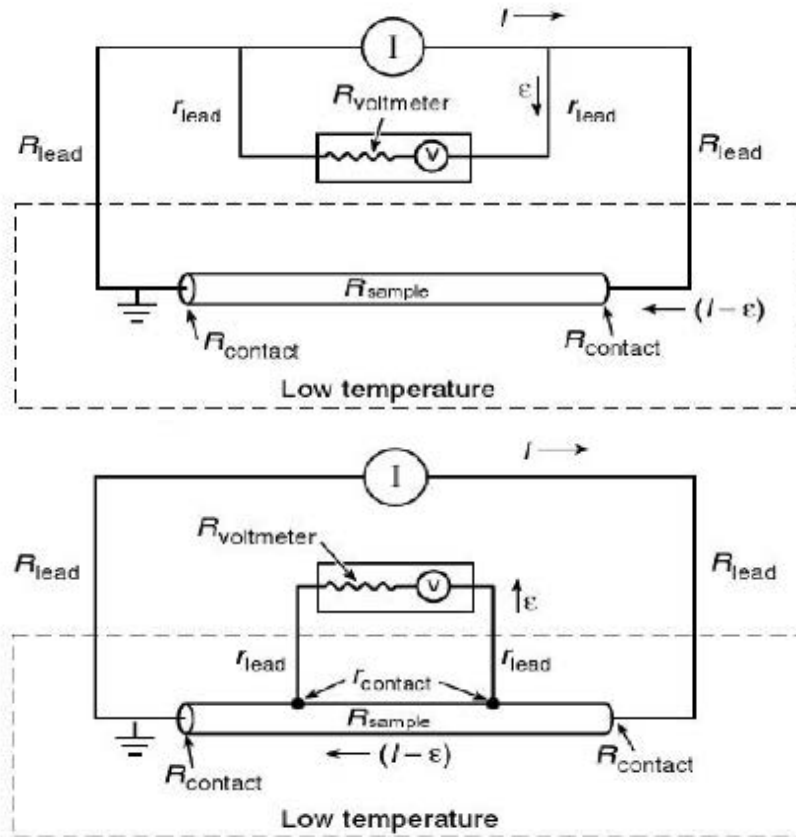


Figure 2.1: Two lead arrangement (top) and four lead arrangement (bottom) for measuring resistance [72].

2.3.4 Heat Capacity

Specific heat measurements can grant significant information about any properties of a material that may change with temperature, particularly at lower temperatures. Specific heat measurements were conducted with the assistance of Dr. Melissa Gooch using the Quantum Design Physical Properties Measurement System (PPMS), with a temperature range from 4.2 K to 300 K and magnetic fields of up to 7 T.

Specific heat is defined as heat capacity per amount of material. Measurements were of solid state samples in a controlled environment of constant pressure.

$$C_p = \left(\frac{dQ}{dT}\right)_p \quad (2.4)$$

The PPMS uses a relaxation technique for the measurement of heat capacity, with a heating period followed by a cooling period of equal duration. Samples are measured on a platform upon a heat capacity puck with a layer of Apiezon N grease providing good thermal contact. After stabilization at the starting temperature, the heater is turned on for a fixed period, followed by the relaxation period. The temperature of the sample, platform, and puck are each monitored for the duration. This data is then compared to a prior measurement (addenda) of the platform with grease, but no sample. The below equations show these calculations where the temperatures are measured directly, and the thermal conductance values are known from standards.

$$C_{platform} \frac{dT_{platform}}{dt} = P(t) - K_{wires}(T_{platform}(t) - T_{puck}) + K_{grease}(T_{sample}(t) - T_{platform}(t)) \quad (2.5)$$

$$C_{sample} \frac{dT_s}{dt} = -K_{grease}(T_{sample}(t) - T_{platform}(t)) \quad (2.6)$$

This model simulates the temperature change due to heat flow from the puck, to the platform, to the sample, assuming non-ideal thermal contact between the puck and the sample holder. If this two tau model fails to find a fit, the simpler one tau model is used, calculating the joint heat capacity of the sample and platform.

$$C_{sample+platform} \frac{dT}{dt} = -K_w(T_{sample+platform} - T_{puck}) + P(t) \quad (2.7)$$

The calculations of the specific heat from the heat capacity assume a given molar mass, thus there can be variations if the real sample is off-stoichiometry. This is most important in the measurement of precise values. For the purposes of this research, the most important features are the transitions which illustrate a change in structure or magnetic ordering, and these are not meaningfully changed. As such, in this context, the precise oxygen content and stoichiometry of samples is not a concern.

Chapter 3

Experimental Results

With so many inconsistent reports of the properties of $PrBa_2Cu_3O_{7-\delta}$ and related compounds, no thorough investigation may be done without first confirming the basic properties. Here this has been done for a variety of preparation techniques that have been reported to grant superconductivity. This includes the solid state method, Pechini method, and aluminum doping for oxidized $PrBa_2Cu_3O_{7-\delta}$ as well as measurements on reduced $Pr_2Ba_4Cu_7O_{15-\delta}$.

No superconductivity was seen. However, I witnessed signs of impurities and measurement artifacts which may have been mistaken for superconductivity by less assiduous researchers in several measurements. Generally speaking, everything reported in this chapter confirms the general picture of the compounds as non-superconducting semiconductors, if not insulators.

One possibility is excluded: no single crystals were synthesized. There is no explanation for why superconductivity would only appear in single crystals, or indeed why single crystals would have significantly different electronic properties than polycrystalline samples aside from the possibility of intrinsic stress or strain playing a large role.

3.1 Solid State Synthesis

The solid state method is the simplest, most common, and arguably the fastest for synthesizing these compounds. Simply mix an appropriate molar ratios of oxides or carbonates containing praseodymium, barium and copper, grinding thoroughly into a fine powder, then repeat the process of calcining, regrinding, and pressing the powder into pellets until samples of the desired quality have been achieved. Calcination is generally performed in an argon atmosphere to reduce the formation of impurities, as with other RBCO compounds. The constituent powders used in this case were Pr_6O_{11} , $BaCO_3$, and CuO .

3.1.1 Structure

The purity of samples produced via the solid state method is directly correlated to how well they are ground and mixed. All samples were manually ground with an agate mortar and pestle. When ground once prior to sintering at 850°C in Argon gas, the initial XRD pattern is rife with impurities, and components which are likely unreacted, though the primary phase is nonetheless easily discerned.

However, after regrinding and recalcining the sample, the pattern improves greatly, though with clear $BaCuO_{2+x}$ impurities. Nor did the pattern change appreciably from there after an oxygen anneal.

3.1.2 Magnetism

As one might expect, the magnetic response for a solid state sample is in no way notable. Limited measurements were done for these samples, but they precisely followed the pattern of those synthesized via the Pechini method, albeit with a higher likelihood of impurity driven anomalies such as a second inflection point below 5 K which is ascribed to $BaCuO_{2+x}$, as seen in Figure 3.3.

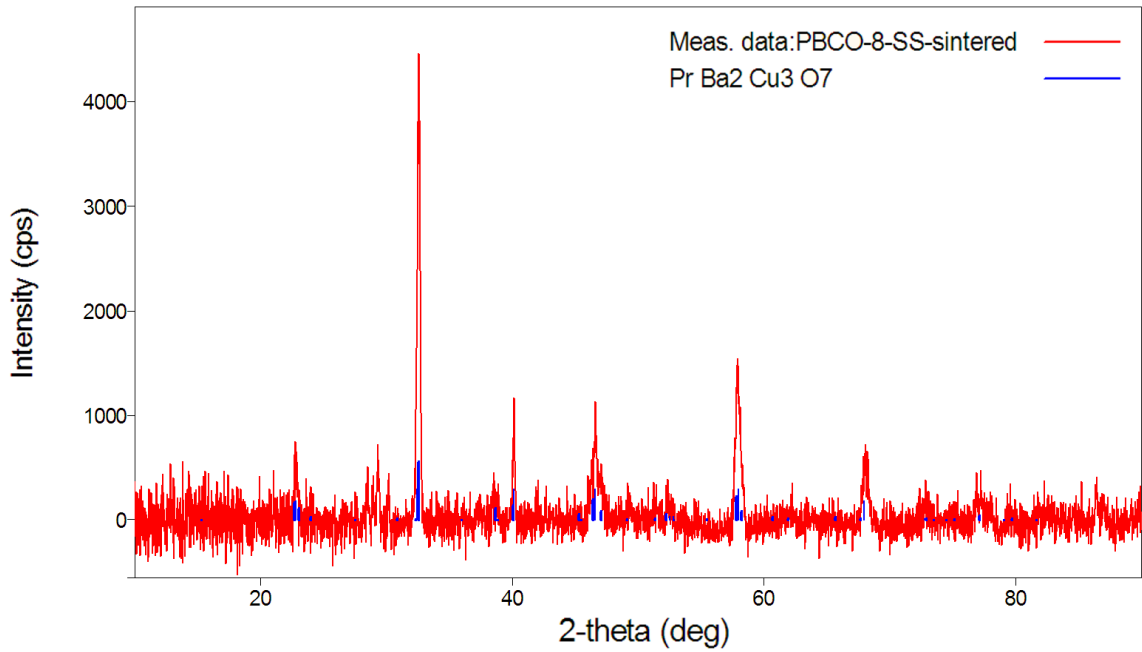


Figure 3.1: Initial XRD Pattern after sintering for sixty hours.

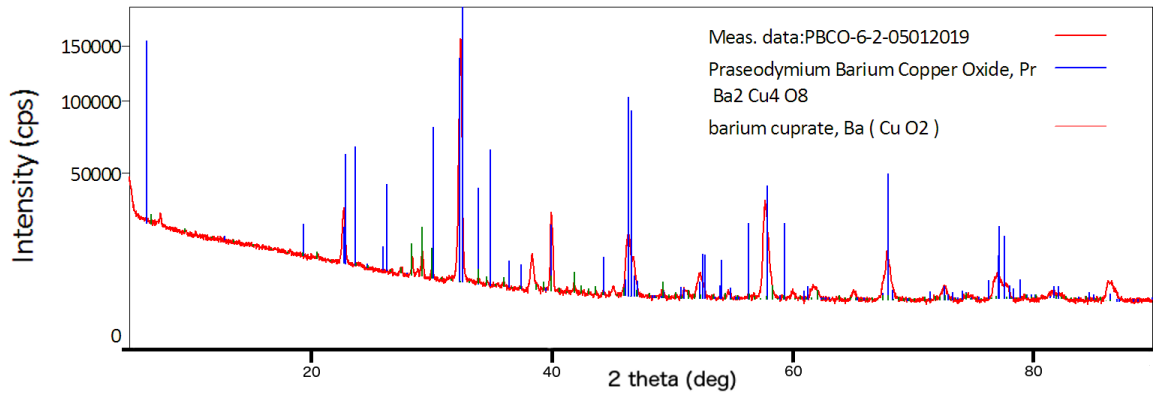


Figure 3.2: XRD pattern after sintering for a total of 120 hours, followed by an oxygen anneal for 72 hours, having been ground and pressed three times.

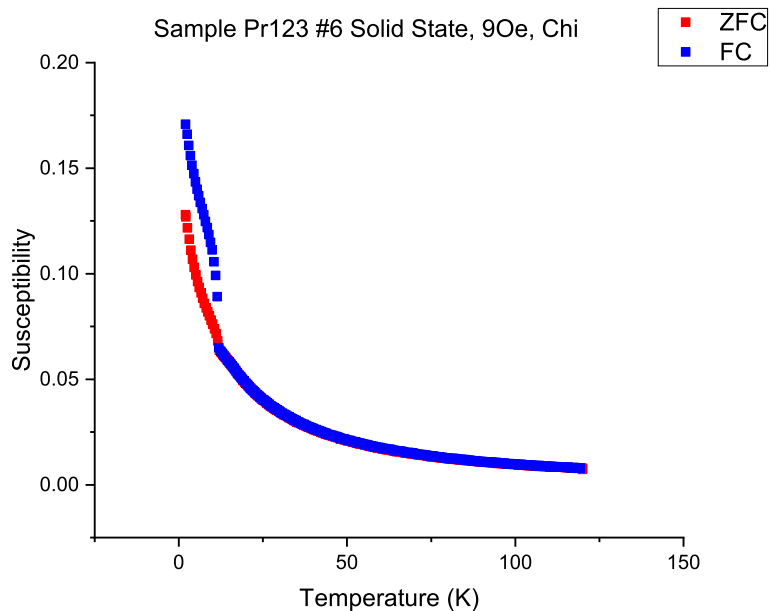


Figure 3.3: Low field MT data for a Pr123 sample synthesized via the solid state method.

3.2 Pechini Method

The Pechini method is a sol-gel synthesis route that utilizes citric acid as a chelating agent to coordinate the cations. The most of the same starting components were used as with the solid state route, though $Pr(NO_3)_3 \cdot 6H_2O$ was used in place of the oxide based on the route used by Araujo-Moreira et al, presumably due to high solubility [24]. The components are dissolved into solution with citric and nitric acids, then ethylene glycol is added as a gelling agent. Finally, the solution is neutralized with ethylene diamine. The solution is then heated to boil off excess water, forming first a gel, then eventually a powder. This powder is first heated to 400° C to ensure it is entirely dry and burn off organic components. The powder is then calcined via the same process as the solid state route. The process is described in full in Chapter 2 of this manuscript.

The ostensible advantage of the Pechini method is that due to being first dissolved into and then precipitated out of a presumably homogeneous solution, the powdered precursors are already well mixed and thus react more completely than manually ground and mixed powders. This leads to higher quality samples with fewer regrinding/recalcining steps.

3.2.1 Structure

Due to the high degree of homogeneity without grinding, the Pechini method yields to fully reacted samples after a single calcine. However, that is not to say that there are no impurities. Both $BaCuO_{2+x}$ and $PrBaO_3$ may form in small quantities. However, regrinding and recalcining may eliminate even those impurities up to the sensitivity of XRD (5%), as can be seen by comparing the XRD patterns after 90 and 200 hours (Fig 3.4).

3.2.2 Magnetism

With high purity samples it is easy to track the change in the Néel temperature of antiferromagnetic $PrBa_2Cu_3O_{7-\delta}$ as the oxygen content is modified, as well as the behavior under varied magnetic fields. Herein I primarily use a particularly well studied and high purity sample (#11), but this has held true for most equivalent measurements. Figure 3.5 shows the sample prior to oxygen anneal, with $T_N \approx 13$ K and $\mu = 3.11\mu_B$.

Fig 3.7 shows that oxygenation appears to remove the low temperature inflection, while moving the Néel transition to 18 K, as has been reported elsewhere. This also changes the magnetic moment to $\mu = 2.88\mu_B$ in keeping with the expected value. When looking at the inverse susceptibility, however, it is clear that the low temperature behavior remains, though it has been suppressed somewhat. It is also clearly visible looking at the first derivative (Fig 3.6; this also assists in pinpointing the AFM transition. The low temperature transition is completely suppressed when the field is increased to 5 T (Fig 3.8 and Fig 3.9). The primary AFM transition, however, remains at 18 K. This remarkable resilience to external field is one of the extraordinary magnetic properties of $PrBa_2Cu_3O_{7-\delta}$ which has yet to be fully explained, but is most likely due to robust long range ordering.

3.2.3 Heat Capacity

In addition to measuring the magnetic properties, heat capacity was also investigated to ensure that no additional phases or transitions were apparent in the sample. Figure 3.10 shows that the oxygenated sample only has a single clear transition. Interestingly,

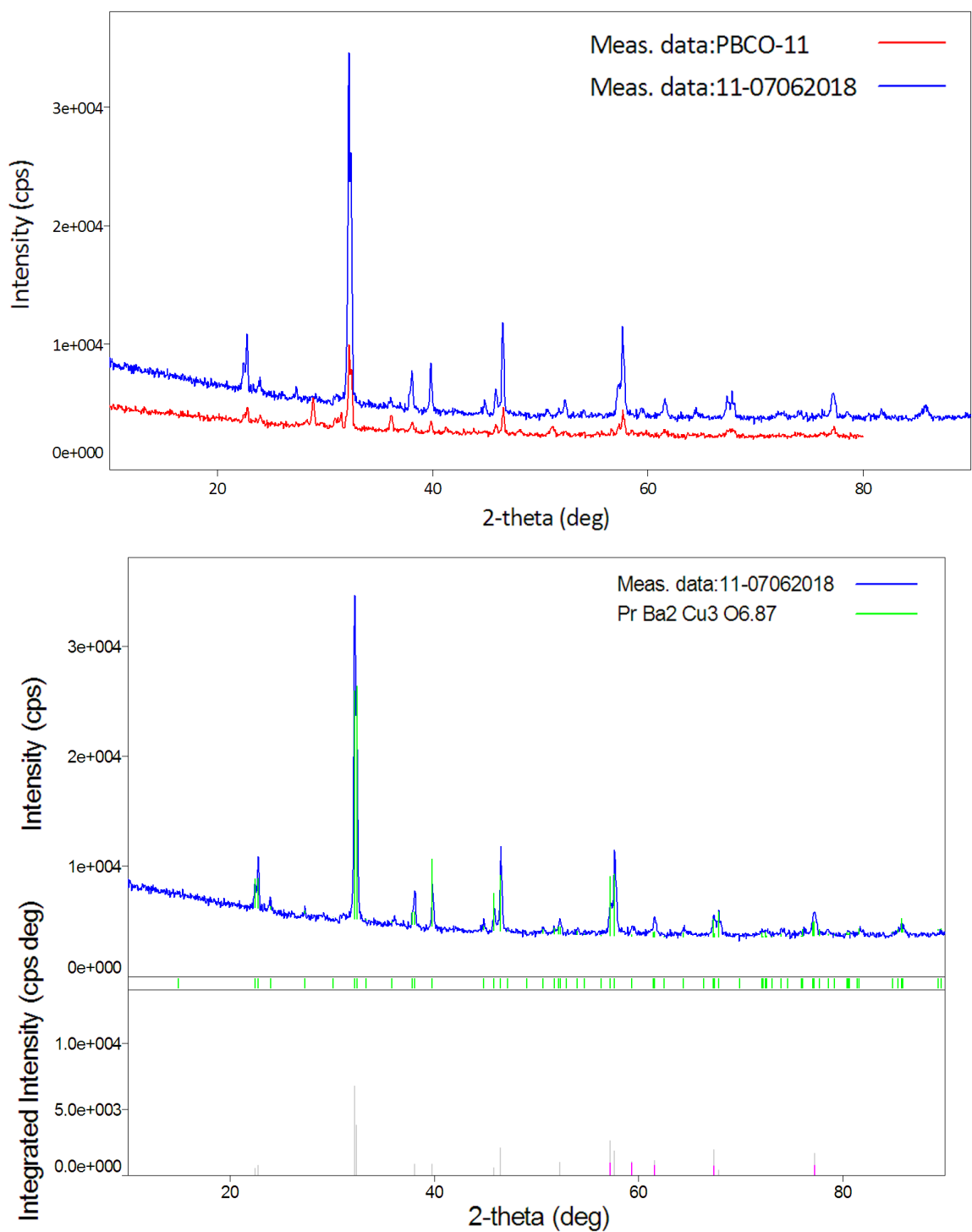


Figure 3.4: (Top) Pechini method synthesized sample comparing patterns after sintering for 90 hours and 200 hours total. After 200 hours, impurity phases are no longer evident. (Bottom) 200 hour sample with peak matching to Pr123.

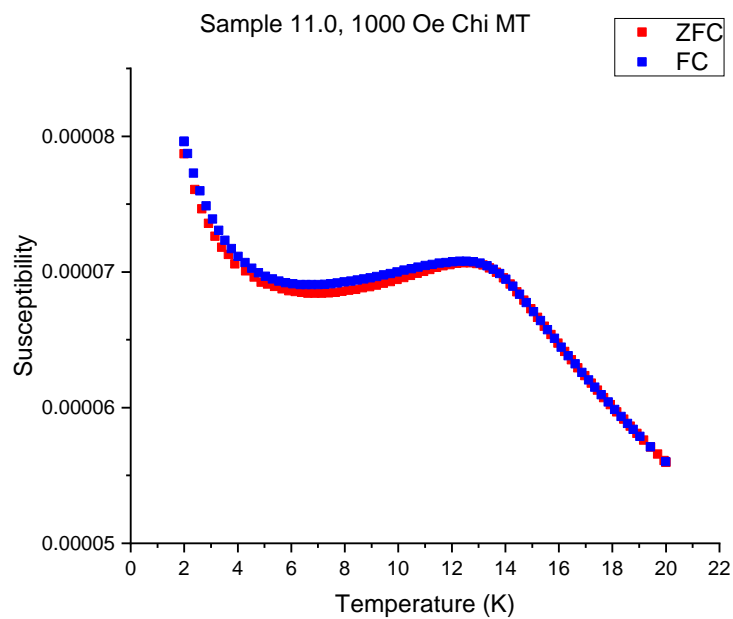


Figure 3.5: Sample 11.0 (reduced) measured under 1000 Oersted. $T_N \approx 13$ K.

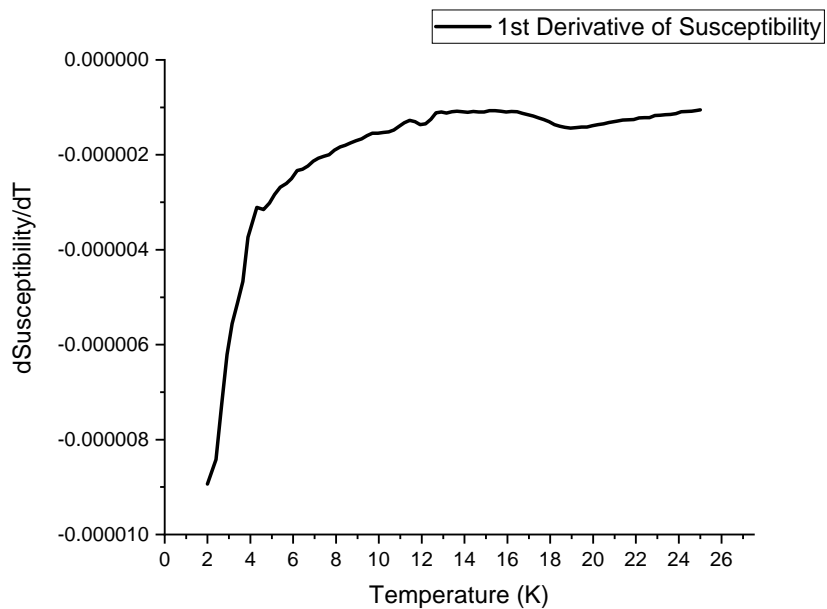


Figure 3.6: First derivative of the susceptibility data shown in Fig 3.7, pinpointing the transitions.

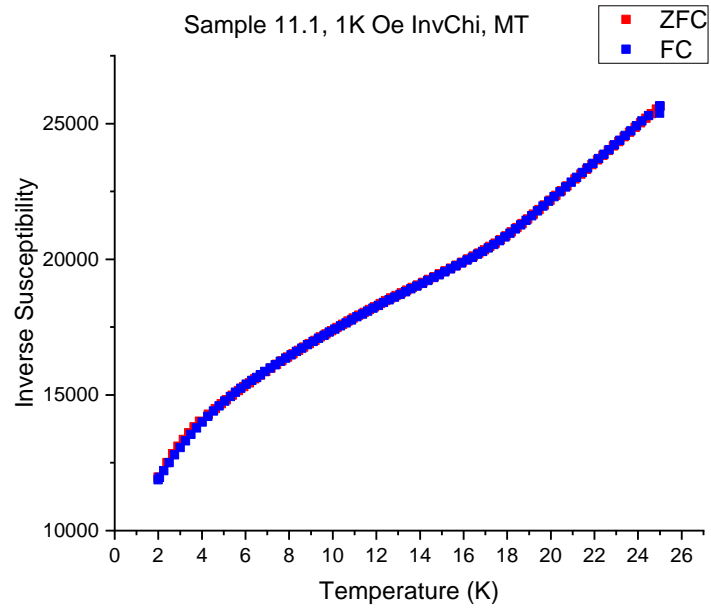
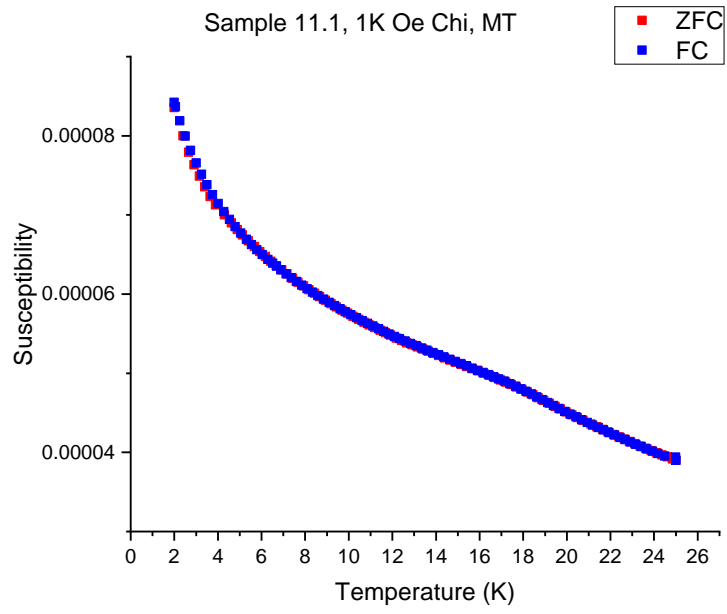


Figure 3.7: Sample 11.1 (oxygenated) measured under 1000 Oersted. $T_N \approx 18$ K. Low temperature transition visible in inverse susceptibility.

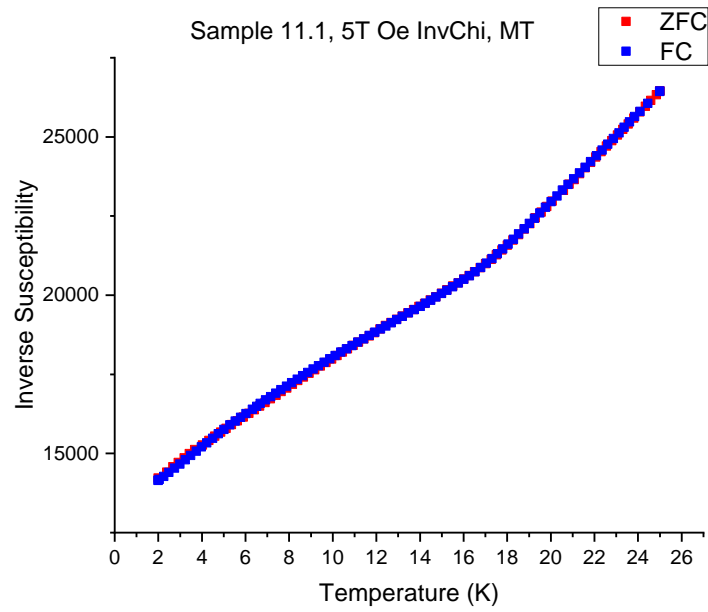
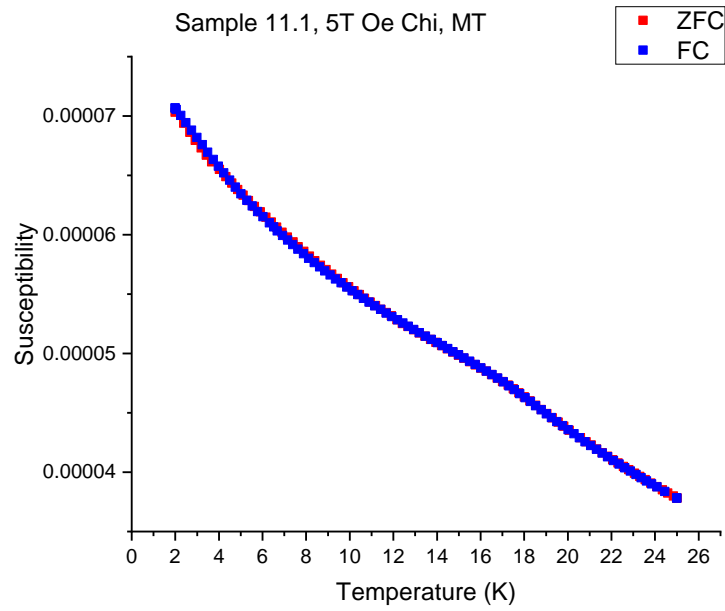


Figure 3.8: Sample 11.1 (oxygenated) measured under 5 Tesla. $T_N \approx 18$ K. Low temperature transition has been completely suppressed.

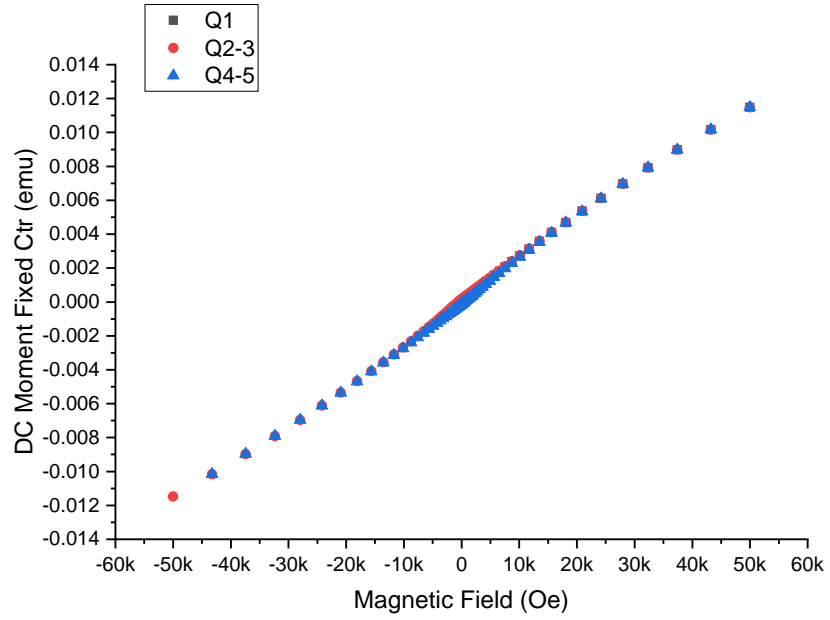


Figure 3.9: MH data for $PrBa_2Cu_3O_{7-\delta}$ showing antiferromagnetism at 5 Kelvin.

while there is a clear lambda transition for the AFM transition at around 18 K, the low temperature change apparent in the MT measurements does not appear.

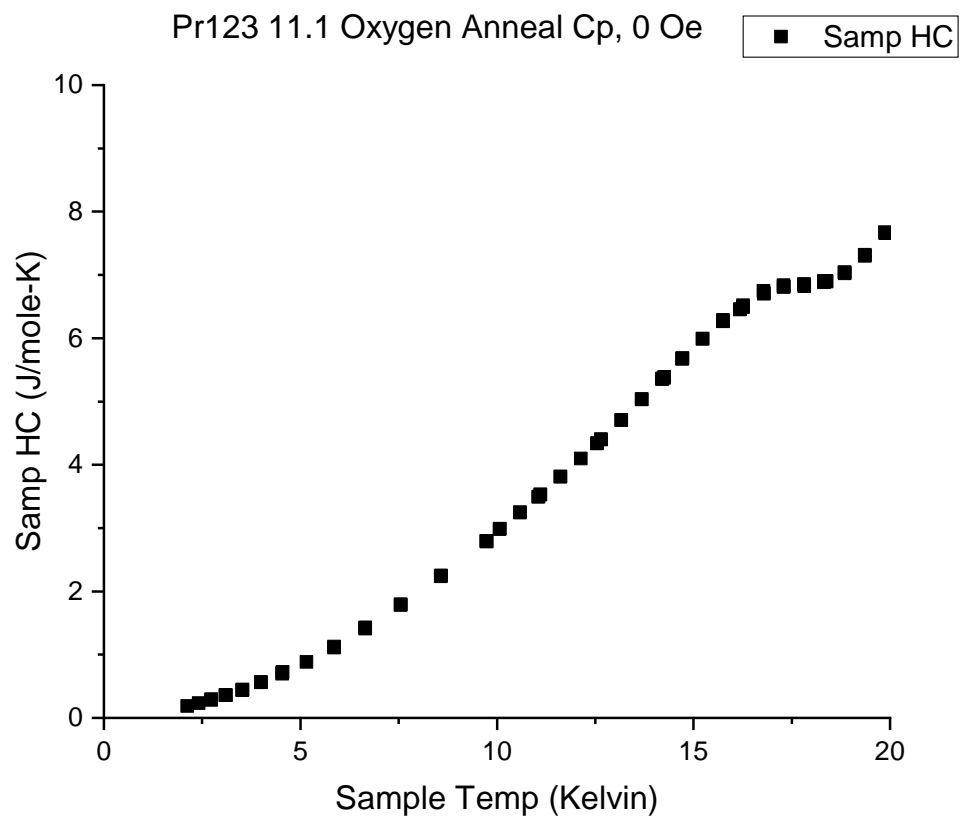


Figure 3.10: Heat capacity measurement under zero field for the oxygenated sample.

3.3 Pr_2BaCuO_5 (Pr211)

An accidental discovery was the formation of Pr211 when $PrBa_2Cu_3O_{7-\delta}$ melts in Argon atmosphere. This was encountered when following the procedure used by Łuszczek et al. [5] for annealing samples in reducing atmosphere at temperatures of over 950° C prior to oxygenation. When mimicking this procedure, it was noticed melting was occurring. When allowed to melt for longer periods of time it was determined from XRD (Fig. 3.11) that Pr211 was forming out of the melt, and was thus responsible for the bizarre magnetic properties witnessed in the samples which underwent that treatment.

3.3.1 Magnetism

The magnetic properties may lend some insight into the behavior of praseodymium relative to yttrium and other rare earths in the perovskites. Notably, Y_2BaCuO_5 has a high temperature ‘spin glass’ transition at 110 K and a low temperature (10-30 K) AFM transition [73]. Unfortunately, the other R211 materials have not been as thoroughly studied as one might hope- for instance, no AC measurements appear to have been made to confirm the nature of the reported spin glass transition.

Figure 3.12 shows the DC MT for a melted Pr123 sample where Pr211 has become the dominant phase. There is a distinct mixed response that is reminiscent of the Kondo effect, and is likely also caused by competing magnetic orders, such as short range ferromagnetic order and long range antiferromagnetic ordering.

We can confirm the presence of FM order by examining MH data around the 12 K inflection point in Figure 3.13.

In order to eliminate the possibility of a spin glass state, AC measurements were conducted as the spin glass transition has a well documented frequency dependence [74, 75]. This sample shows none across three orders of magnitude, indicating that it is not a spin glass (Figure 3.14).

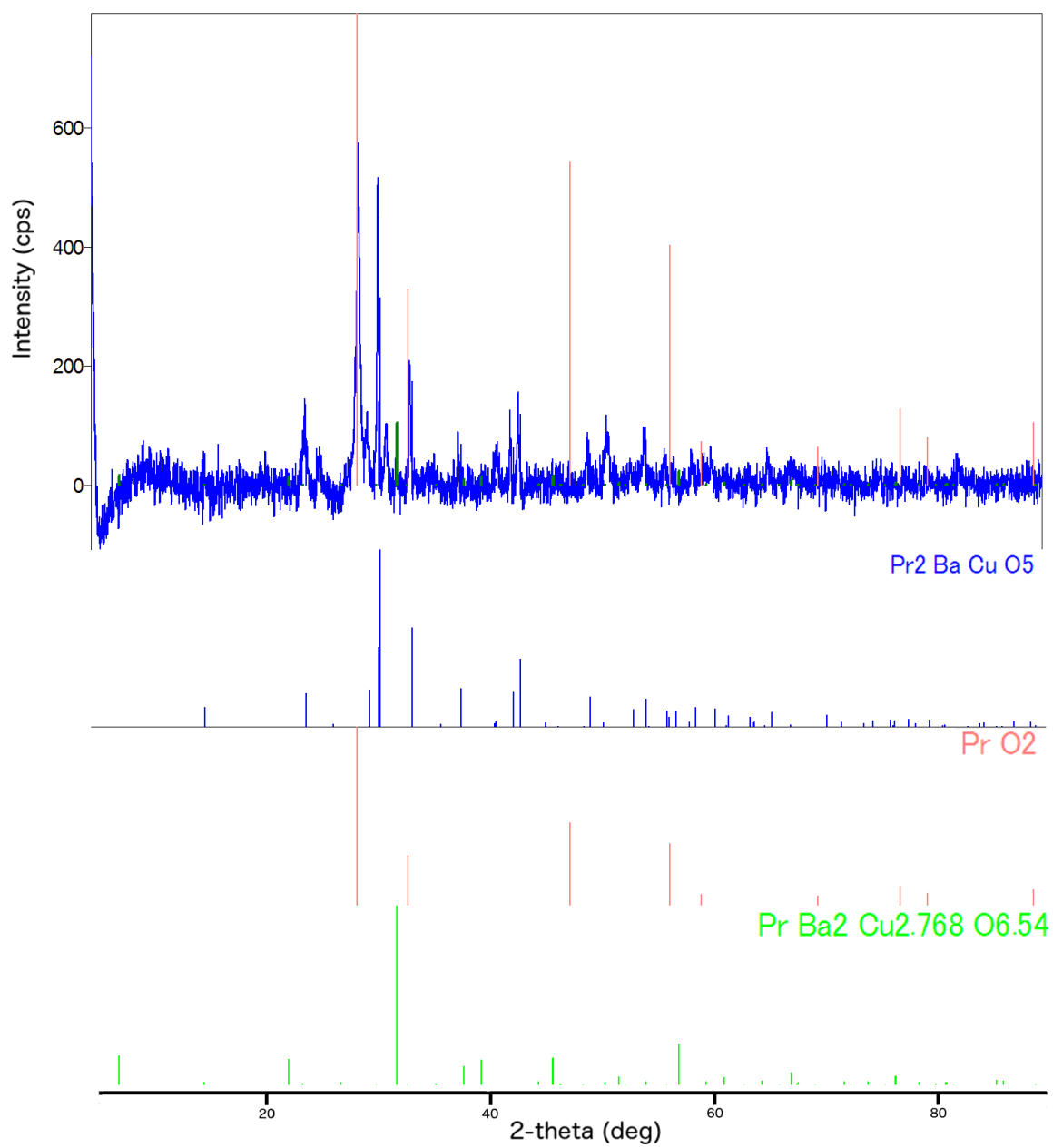


Figure 3.11: Melted Pr123 decomposes into praseodymium oxide, Pr₂O₃, and other compounds likely including copper oxide and barium cuprate.

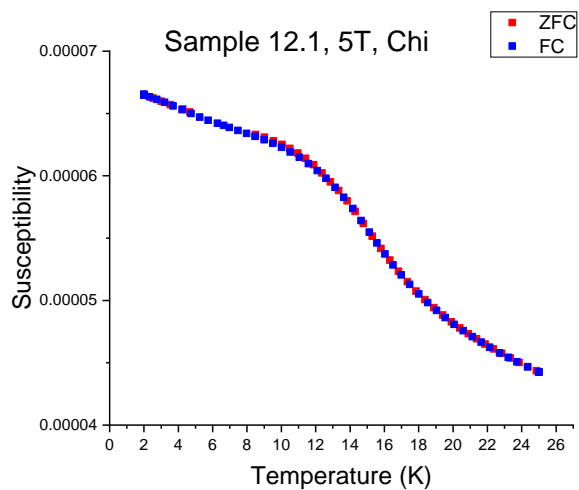
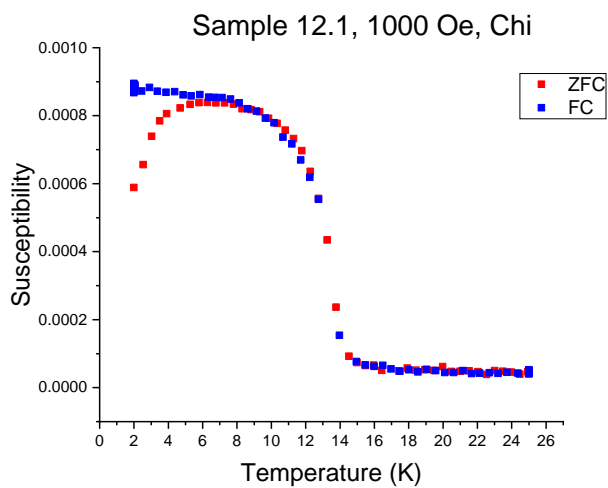
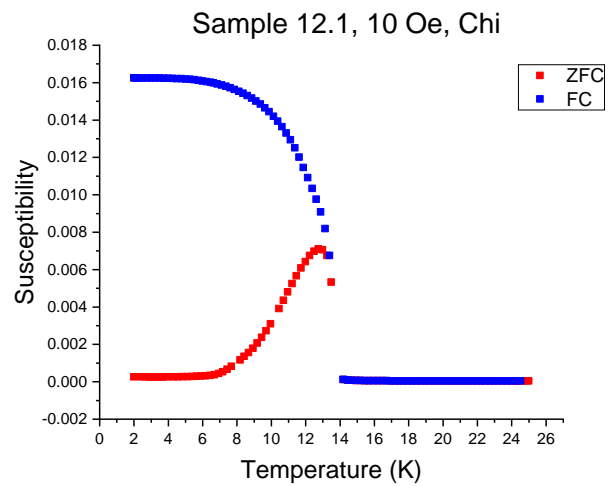


Figure 3.12: Competing AFM/FM interactions over long/short ranges in Pr211. MT at three different fields shown. No higher temperature transitions are seen up to 300 K.

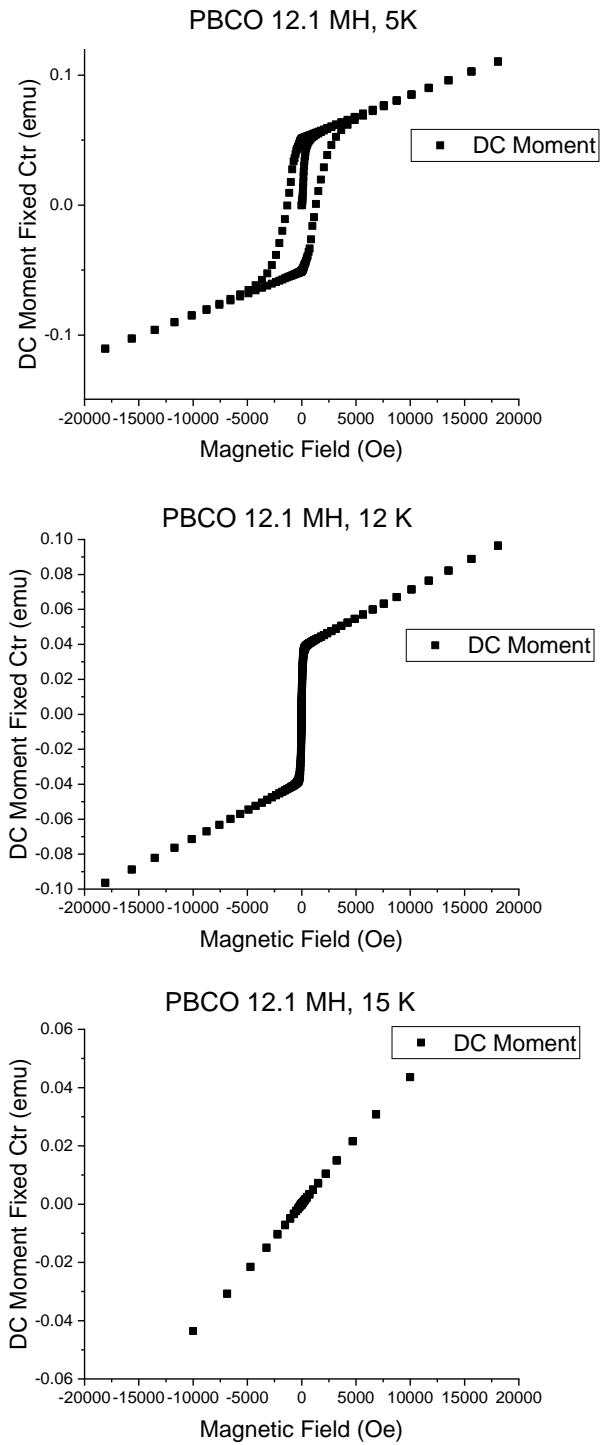


Figure 3.13: At 5K, there is a clear FM hysteresis, with a coercive field around 0.25 T. At 12 K, where there is an inflection point in my low field MT data, one can still see the clear FM moment, but saturation occurs immediately. At 15 K, above the transition, the FM moment vanishes entirely.

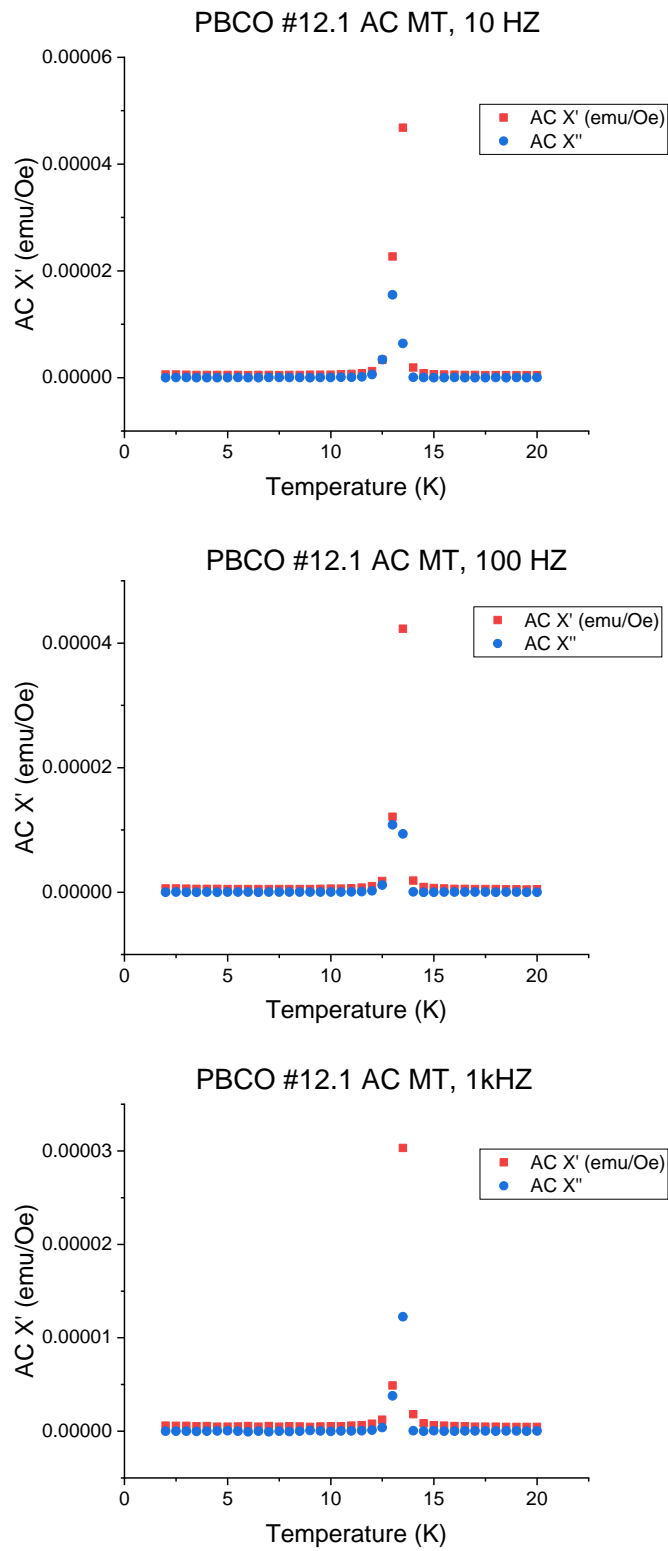


Figure 3.14: No frequency dependence of the magnetic transition from 10Hz-1000Hz.

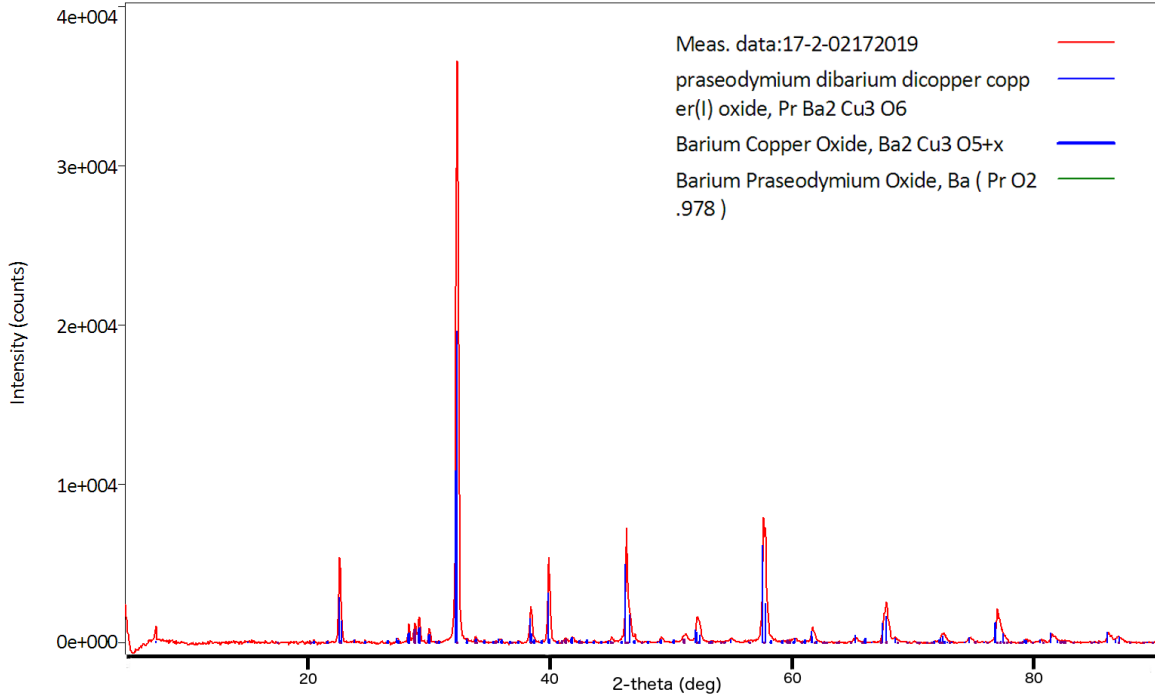


Figure 3.15: 10% replacement of copper by aluminum, normal assortment of impurities.

3.4 Al Doping

Luszczek *et al.* [5] also found that the crucible used for synthesis was important for generating superconductivity. Superconductivity only appeared in single crystals prepared in alumina (Al_2O_3) crucibles, which were then found to have significant aluminum contamination. Thus I tested several levels of aluminum substitution for copper (10, 20 and 30%) to see if this notably altered the properties. The Pechini method was used for synthesis, using $Al(NO_3)_3 \cdot 9H_2O$ for the aluminum bearing precursor as alumina is not soluble.

3.4.1 Structure/Purity

Examining the XRD data, when 10% or 20% of copper is replaced with aluminum, the aluminum appears to mostly be integrated into the crystal structure as no aluminum bearing impurities appear in the XRD pattern (Figures 3.15 and 3.16). At 30%, distinct aluminum related impurities appear, indicating that saturation has been reached (Fig. 3.17).

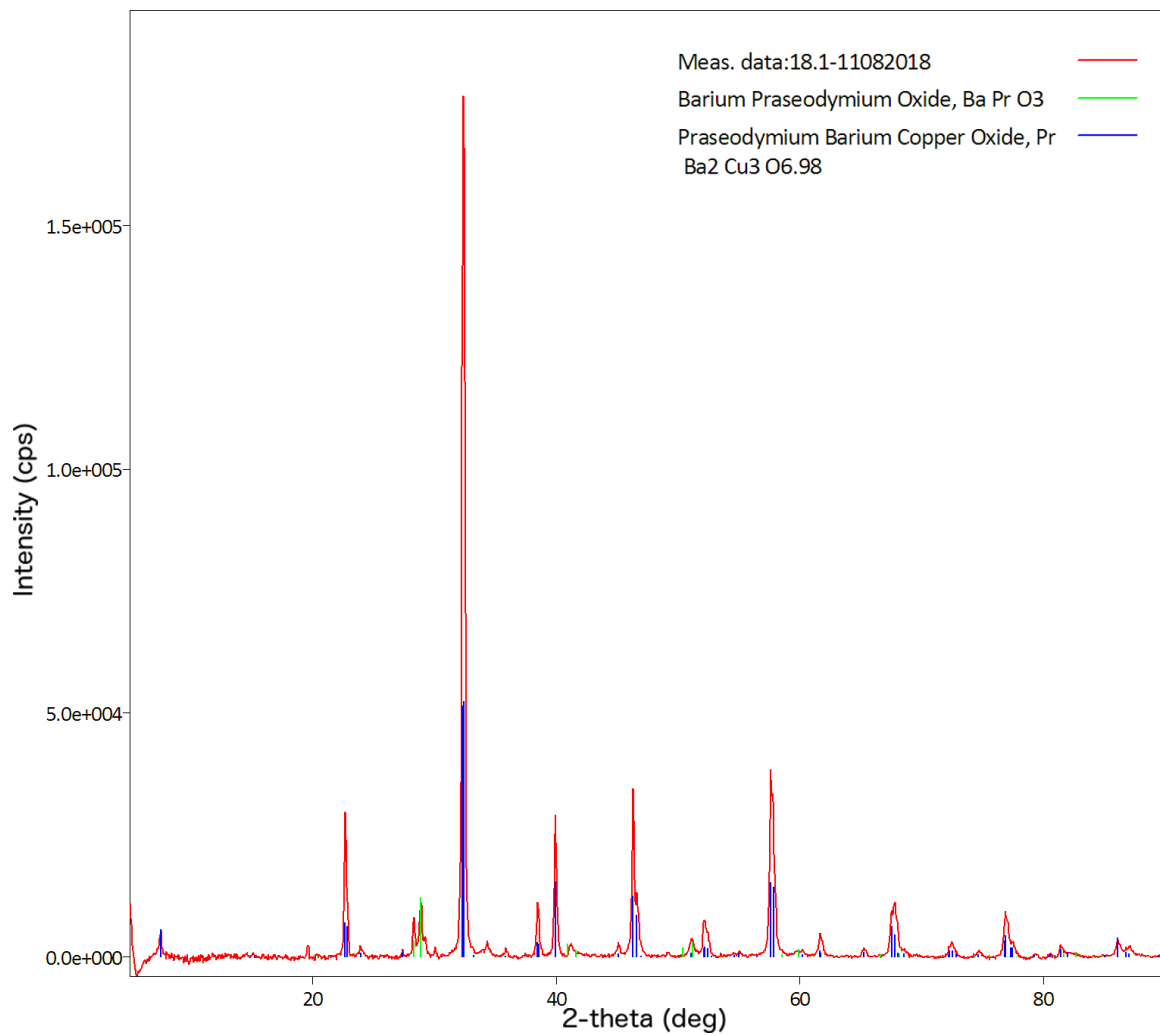


Figure 3.16: 20% replacement of copper by aluminum, ordinary $PrBaO_3$ impurities present.

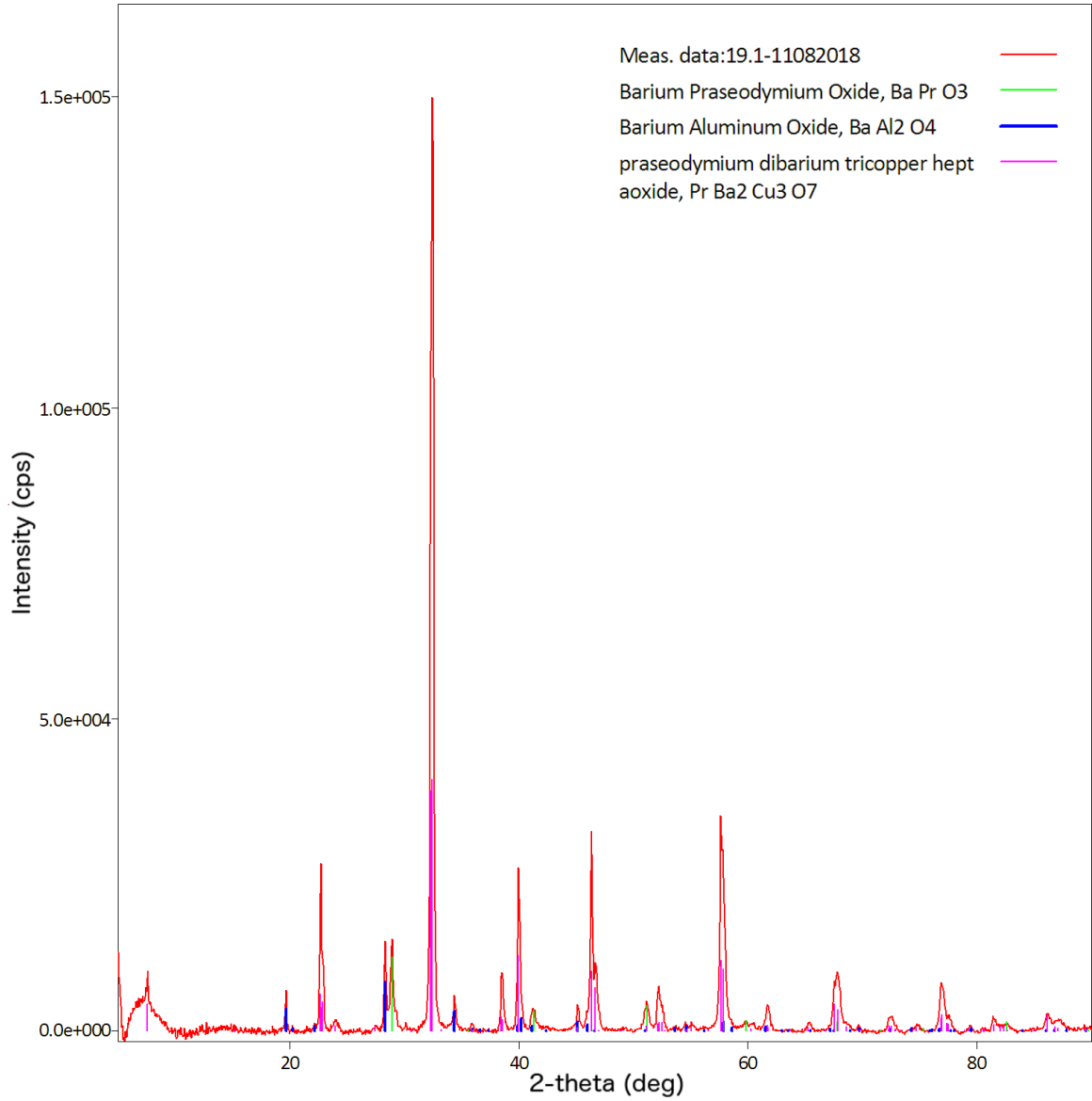


Figure 3.17: 30% replacement of copper by aluminum, includes Al based impurity $BaAl_2O_4$.

3.4.2 Magnetization

There are no smoking guns in the magnetization data unless the oxygenated curves, shown below, are considered. There a surprise is found- the oxygenated curves are not distinctly different from the original reduced samples. Rather than oxygenation increasing the Néel temperature, it remains fixed around, or even slightly below, 12 K, whereas fully oxygenated Pr123 has a $T_N \approx 17 - 18$ K. The exact cause of this is unclear, but it is most likely due to the aluminum inhibiting oxygen uptake rather than dramatically changing the magnetic properties.

I also recorded μ for the samples as the aluminum content is increased. Perhaps unsurprisingly, given the apparent impact on oxygen uptake, these values are close to the value for reduced Pr123 to begin with, though as the aluminum content increases, μ decreases nearly to the expected value: $\mu_{Al=10\%} = 3.13$, $\mu_{Al=20\%} = 3.02$, $\mu_{Al=30\%} = 2.93$ (Figures 3.18, 3.19, and 3.20). Clearly there are multiple effects in play, likely including impurity phases. As such, these differences are insufficient to draw any strong conclusions about the potential role of Al in creating superconductivity in Pr123 other than the fact that superconductivity was not seen. There may have been some other factor tied to Łuszczek *et al.*'s result [5], such as yttrium contamination of the crucibles from prior usage, which cannot reliably be reproduced or speculated about.

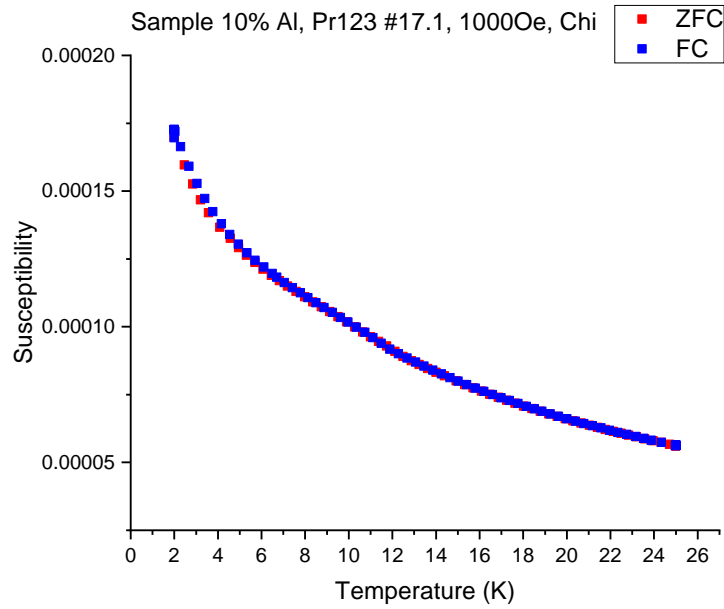


Figure 3.18: 10% replacement of copper by aluminum, less distinct AFM transition at a lower temperature (appears around 10 K vs 12 K for undoped).

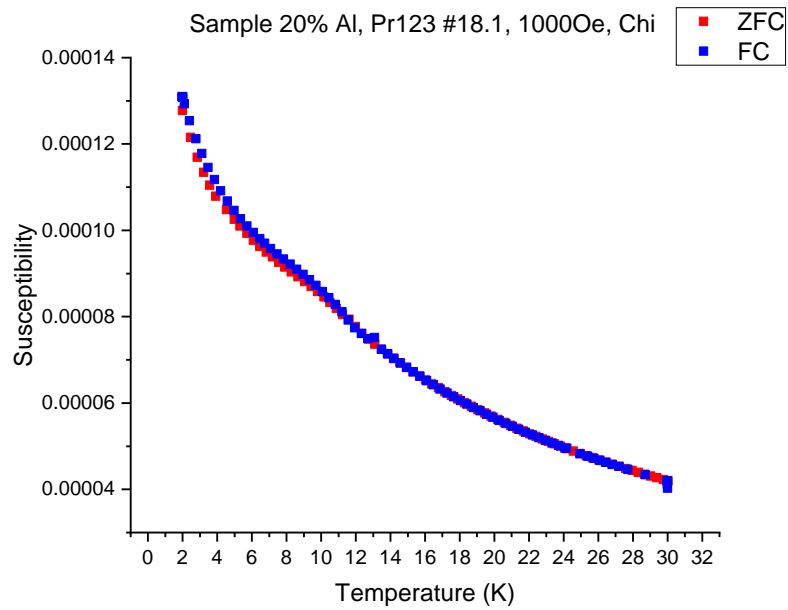


Figure 3.19: 20% replacement of copper by aluminum, further suppression of T_N to around 9 K.

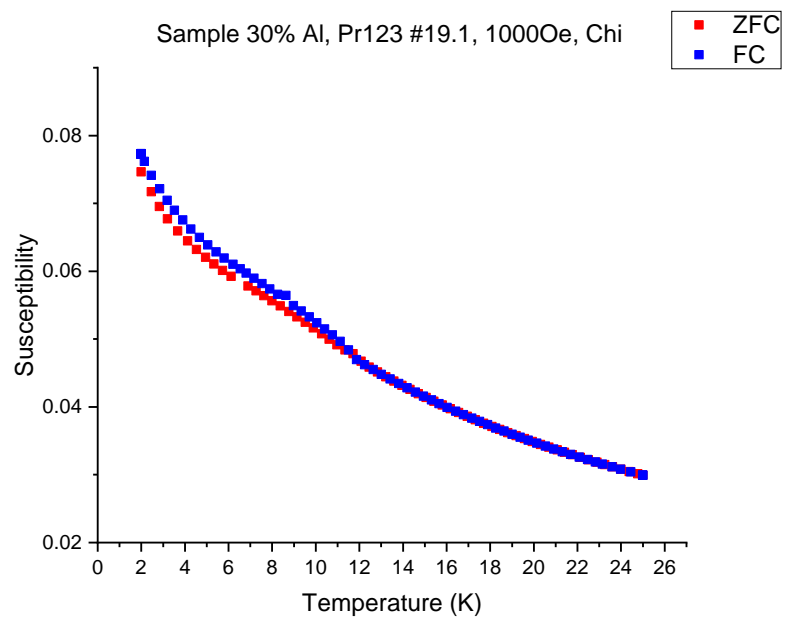


Figure 3.20: 30% replacement of copper by aluminum, includes Al based impurity $BaAl_2O_4$, but does not seem to suppress T_N below 12 K.

3.5 $Pr_2Ba_4Cu_7O_{15-\delta}$

Superconductivity in $Pr_2Ba_4Cu_7O_{15-\delta}$ has been reported separately from superconductivity in $PrBa_2Cu_3O_{7-\delta}$, with different T_c and behavior under pressure. Interestingly, there are discrepancies not only in the presence or absence of superconducting properties, but also in the basic magnetic properties. Under atmospheric pressure it has not been demonstrated that commensurate Pr247 or Pr124 phases exist. Instead, it appears that there is an incommensurate structure where single and double copper oxygen layers appear without long range order. This differs from the interpretation of Hagiwara *et al.* [76] who reported superconductivity in the compound, but is supported both by their reported TEM results and my thermal measurements in the next chapter. It also helps explain many of the discrepancies seen.

3.5.1 Structure

In theory, crystalline $Pr_2Ba_4Cu_7O_{15-\delta}$ should be distinguishable from $PrBa_2Cu_3O_{7-\delta}$ due to different XRD peaks at low angles. The effective addition of another copper oxygen layer to every other cell impacts the (010) reflections, and manifests as a peak at 7.0° vs 6.5° for Pr123 and 7.5° for Pr124. This is not what is seen in Figure 3.21, however. Across the vast majority of my samples of both Pr123 and Pr247, either there is no peak significantly above the level of the background, or there is a peak at 7.5. On the one hand, the peak is sufficiently broad that it includes both lower angle peaks, but the pinnacle is distinctly 7.5, which also matches an impurity peak for $BaPrO_3$.

3.5.2 Magnetism

What impact does that additional copper oxygen layer have on the magnetic properties? There's debate in the literature as to whether or not Pr247 has any AFM transition at all, or whether it exhibits the same transition as Pr123 and Pr124. For it not to would be nonsensical- it should have some combination of the properties exhibited by the single and double copper oxygen chains.

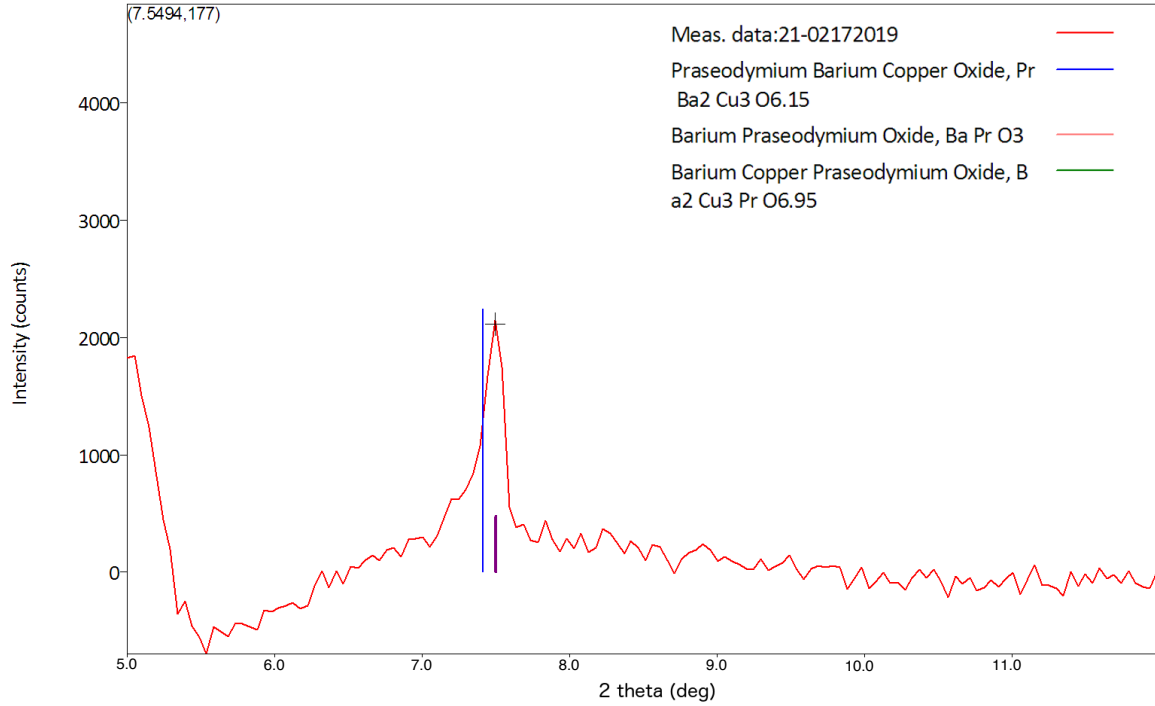


Figure 3.21: Low angle image showing a peak at 7.5° for a Pr247 sample.

The transition is present, but it is more or less evident depending on the sample and the field used. Note how the transition in the reduced sample is readily evident at 10 Oe (Fig. 3.22) but imperceptible at 1000 Oe (Fig. 3.23)

As such it would not be unreasonable to conclude that the transition seen in these Pr247 samples is in fact due to an impurity phase, namely $PrBaO_3$, which has a similar T_N . Except that in an unreduced sample, $T_N \approx 18$ K, which is well above what has ever been reported for the impurity, but expected for fully oxygenated Pr123 (Fig. 3.24).

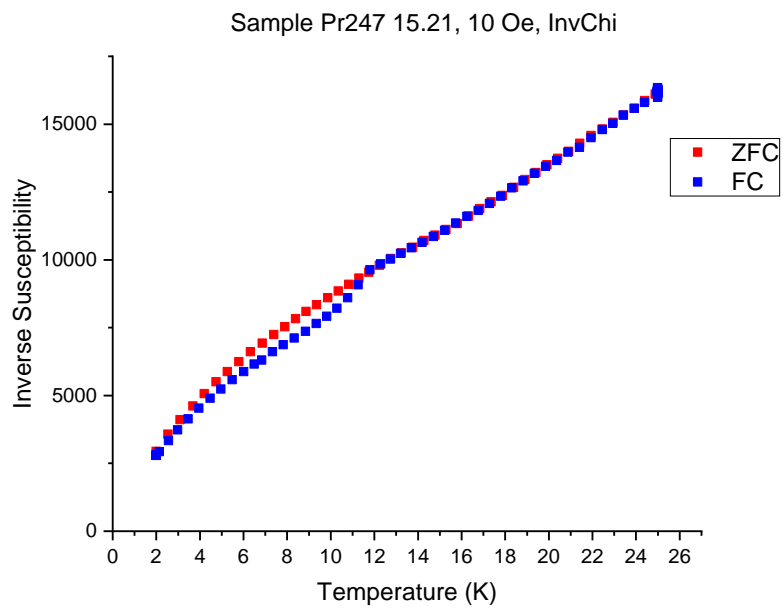
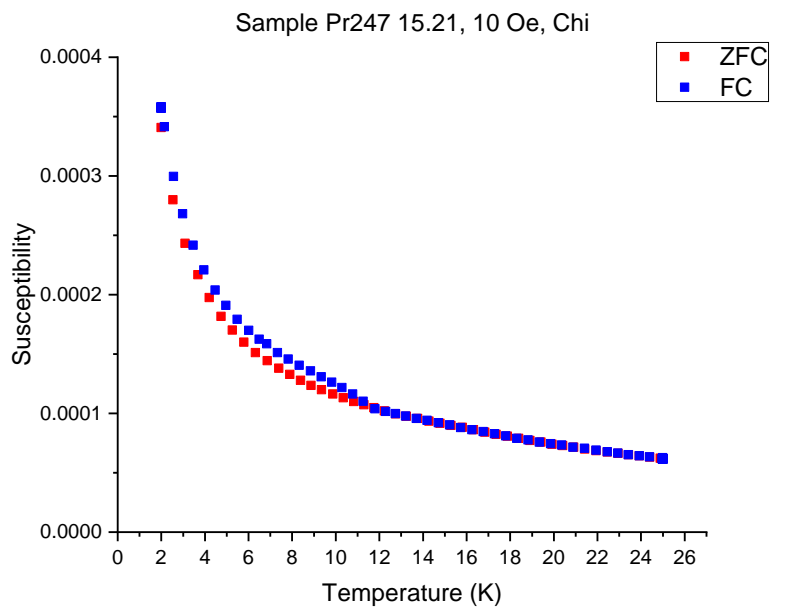


Figure 3.22: MT at 10 Oe the reduced Pr247 sample 15.2, with clear AFM transition at $T_N = 12$ K.

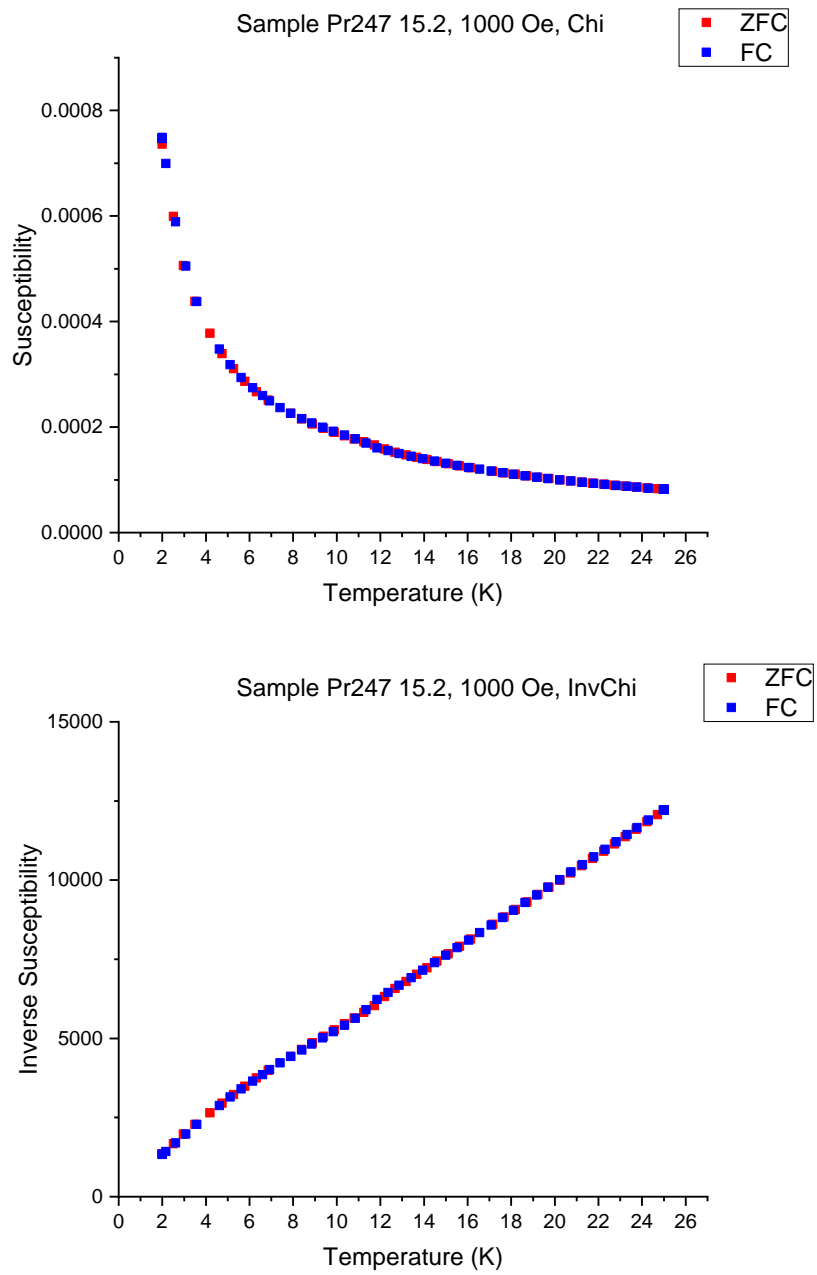


Figure 3.23: MT at 1000 Oe for a the reduced Pr247 sample 15.2, with no visible T_N .

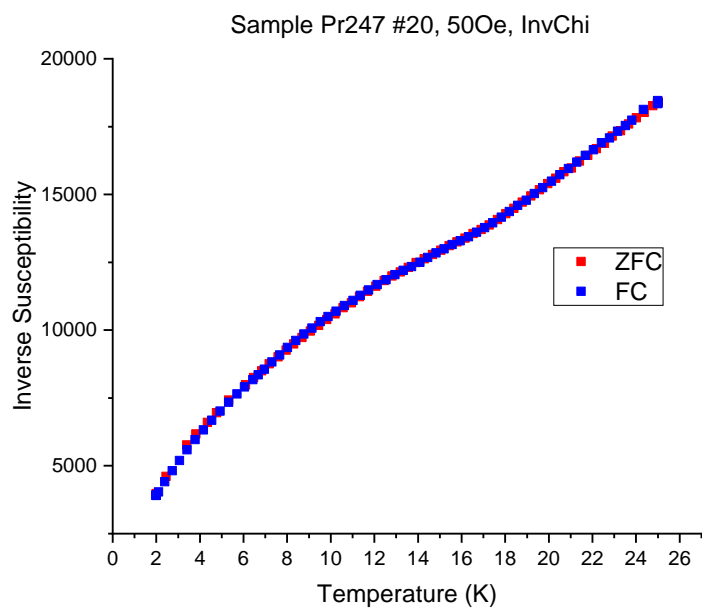


Figure 3.24: MT at 50 Oe for Pr247 sample 20, with $T_N \approx 18$.

Chapter 4

Phase Diagram and Transitions

Having replicated the synthesis conditions used by those who have reported superconductivity under a variety of different conditions and found them lacking, the next step is to explore more of the Pr-Ba-Cu-O phase diagram. If a superconducting phase exists, it clearly requires very specific synthesis conditions. There is also a clear hole in the literature: the phase diagram for the system has not been studied under atmosphere, but all of the potential superconducting results in the system required either synthesis in a reducing or oxidizing atmosphere.

Additionally, there are a number of published claims which are not yet verified. For example, Hagiwara *et al.* claim that Pr124 and Pr247 are distinctly synthesized at temperatures only a few degrees apart under otherwise identical conditions - except for the stoichiometric ratio of the chemical composition, of course [7]. These are testable claims. Unless a sample is completely reacted- which is unlikely given the fact that even the best polycrystalline samples have been shown to have impurity phases present- the formation temperature should appear in DSC data.

4.1 $PrBa_2Cu_3O_{7-\delta}$ in air

As a baseline, $PrBa_2Cu_3O_{7-\delta}$ in air was measured. This is the only measurement for the family which has been previously published, though not at high temperatures that

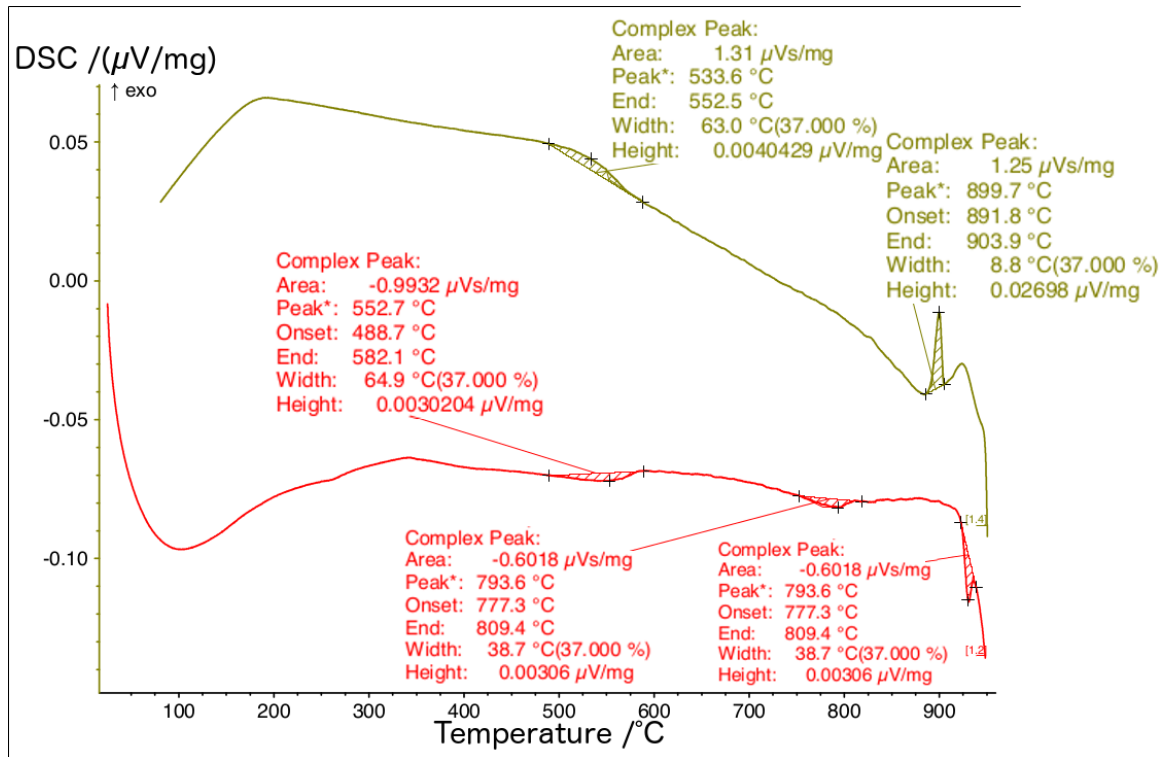


Figure 4.1: DSC measurement of Pr123 sample in air. Two reversible transitions at 552 $^{\circ}$ C and 930 $^{\circ}$ C. Irreversible transition at 793 $^{\circ}$ C, and apparent melting at about 920 $^{\circ}$ C, ascribed to a $PrBaO_3$ impurity phase.

I am aware of. The DSC data for this is shown in Figure 4.1. This shows a pair of reversible transitions, one of which appears to occur amid the melting of another phase, and one irreversible transition. The formation temperature of $PrBa_2Cu_3O_{7-\delta}$ is visible in the irreversible transition peaking at 793.6 $^{\circ}$ C. Despite this sample having been previously sintered and calcined at 850 $^{\circ}$ C multiple times, some impurity phases remain as is shown in the electron probe micro analyzer (EPMA) data (Fig. 4.3 and Table 4.1). The both reversible transitions approximately match those previously reported for $PrBaO_3$, despite none being indexed in XRD measurements on this sample (Fig. 4.2) [77].

The maximum temperature measured was 950 $^{\circ}$ C in order to avoid melting, which has been established to occur at 971 $^{\circ}$ C in air. Thus the endothermic event occurring just below 950 $^{\circ}$ C, due to its magnitude, is assumed to be the partial melting of an impurity phase. But is there a chance that this reversible transition is actually a transition of the bulk that might lead to superconductivity?

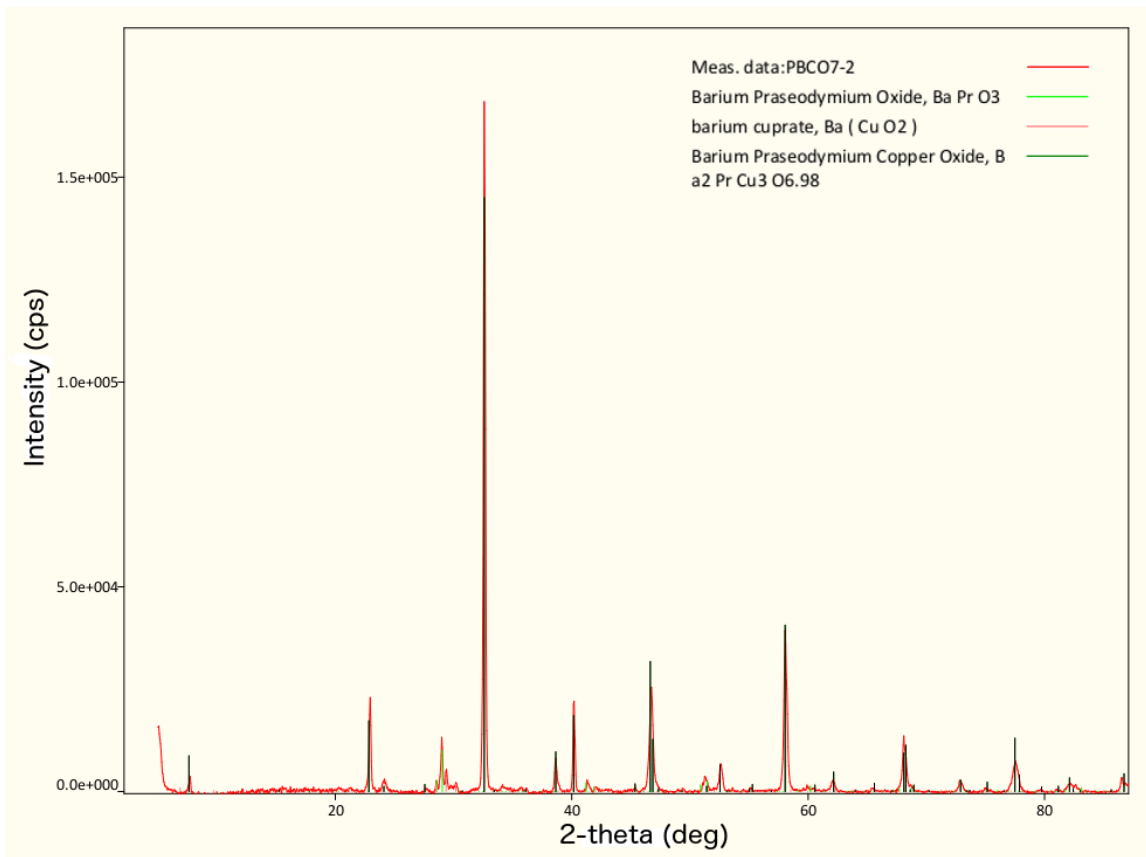


Figure 4.2: XRD for the sample measured via DSC/TGA. $BaCuO_{2+x}$ peaks do not appear, though their locations are included for reference. $PrBaO_3$ peaks clearly present. Both can be found via EPMA.

Pt#	Pr	Ba	Cu	Al	O	Total
0	6.302	14.308	23.413	0.1610	55.816	100.000
1	7.758	14.016	22.994	0.1594	55.073	100.000
2	10.732	18.752	27.575	0.7966	42.145	100.000
3	7.868	13.417	21.311	0.5638	56.840	100.000
4	12.247	20.580	32.400	0.0000	34.773	100.000
5	11.689	22.262	25.668	3.889	36.491	100.000
6	8.134	13.405	22.699	0.2083	55.554	100.000
7	8.362	15.254	24.049	0.0000	52.335	100.000
8	7.893	14.194	23.551	0.2352	54.127	100.000
9	12.241	15.970	16.205	0.0626	55.523	100.000
10	7.996	14.252	23.404	0.3540	53.994	100.000
11	8.366	15.148	21.945	0.0366	54.504	100.000
12	7.904	15.215	19.944	0.0000	56.937	100.000
13	7.801	14.788	23.167	0.3971	53.846	100.000
14	5.252	18.092	27.294	0.4546	48.907	100.000
15	9.509	14.337	21.030	0.4531	54.671	100.000
16	7.784	14.946	20.041	0.5234	56.706	100.000
17	6.655	12.709	19.767	0.1554	60.714	100.000
18	0.7068	18.490	24.062	0.6129	56.128	100.000
19	6.112	15.926	23.694	0.6779	53.590	100.000
20	8.169	14.886	23.673	0.6145	52.657	100.000
21	18.690	17.932	1.5193	0.8015	61.058	100.000
22	15.924	18.665	5.779	0.7953	58.837	100.000

Table 4.1: Atomic proportions measured via EPMA on Pr123 sample after it was used for DSC in air. The vast majority of locations approximate stoichiometric Pr123, with several appearing to contain either $BaCuO_{2+x}$, $PrBaO_3$ or some combination of impurity and primary phase. Aluminum is checked for to see if the crucible contaminated the sample either during calcination or the measurement, but is only appears in a significant quantity at a single point which could not be reproduced.

In order to answer that question, which would not conflict with some of the heat treatments used in literature that reportedly resulted in superconductivity, a sample was annealed at 950° C and quenched in oil, but no superconductivity was detected with MT measurements down to 2 K, the results of which matched those reported in the previous chapter for Pr123.

Notably, there are no separate irreversible transitions for Pr124 or Pr247, though as this measurement was conducted in air rather than oxygen, none were expected.

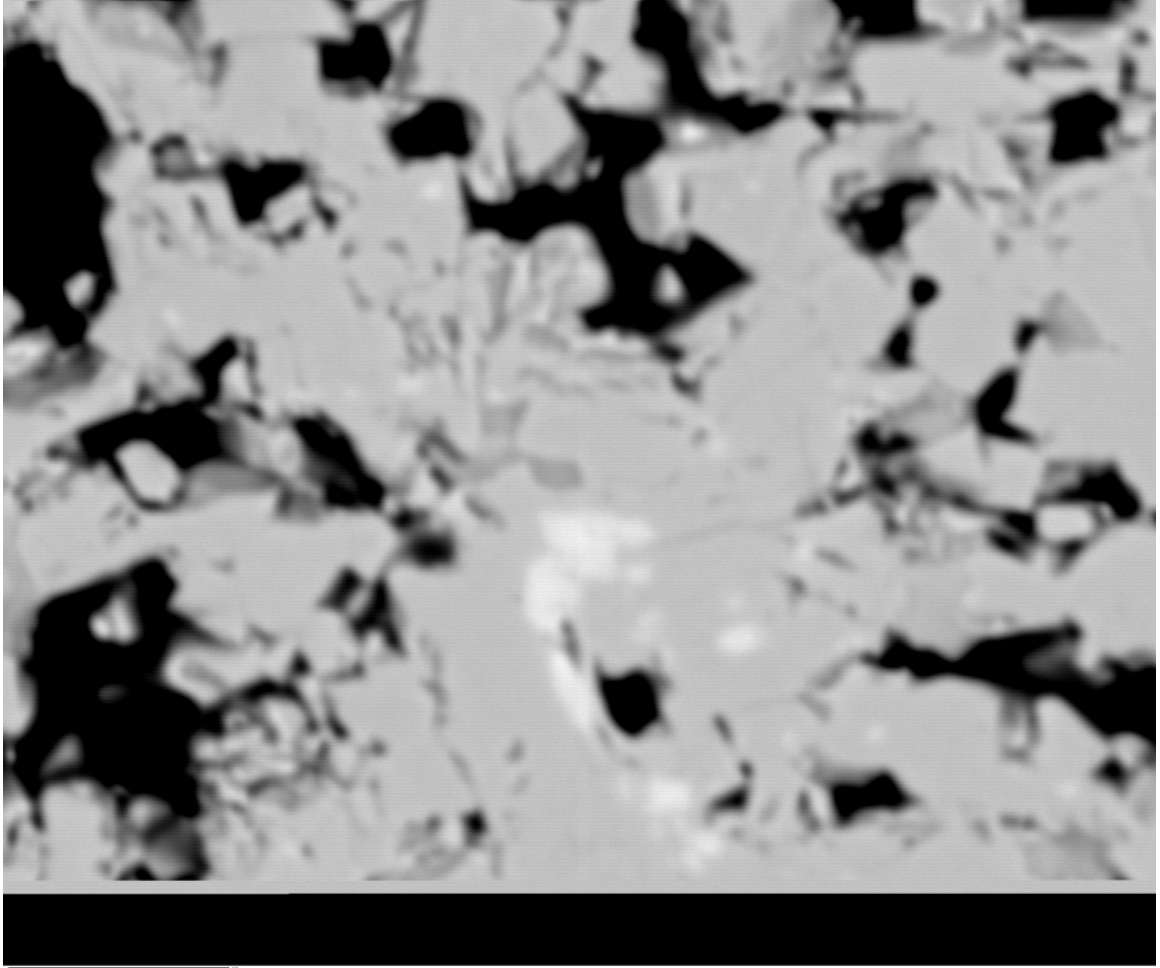


Figure 4.3: EPMA image of the sample used for DSC measurement. Light patch at center-bottom is a $PrBaO_3$ rich region. Darker patches scattered throughout, including above and to the left of the light patch are $BaCuO_{2+x}$ regions. Line along the bottom indicates 10 microns. Impurities predominantly appeared in a few locations along the surface, very rarely found in imaging of the cross sections.

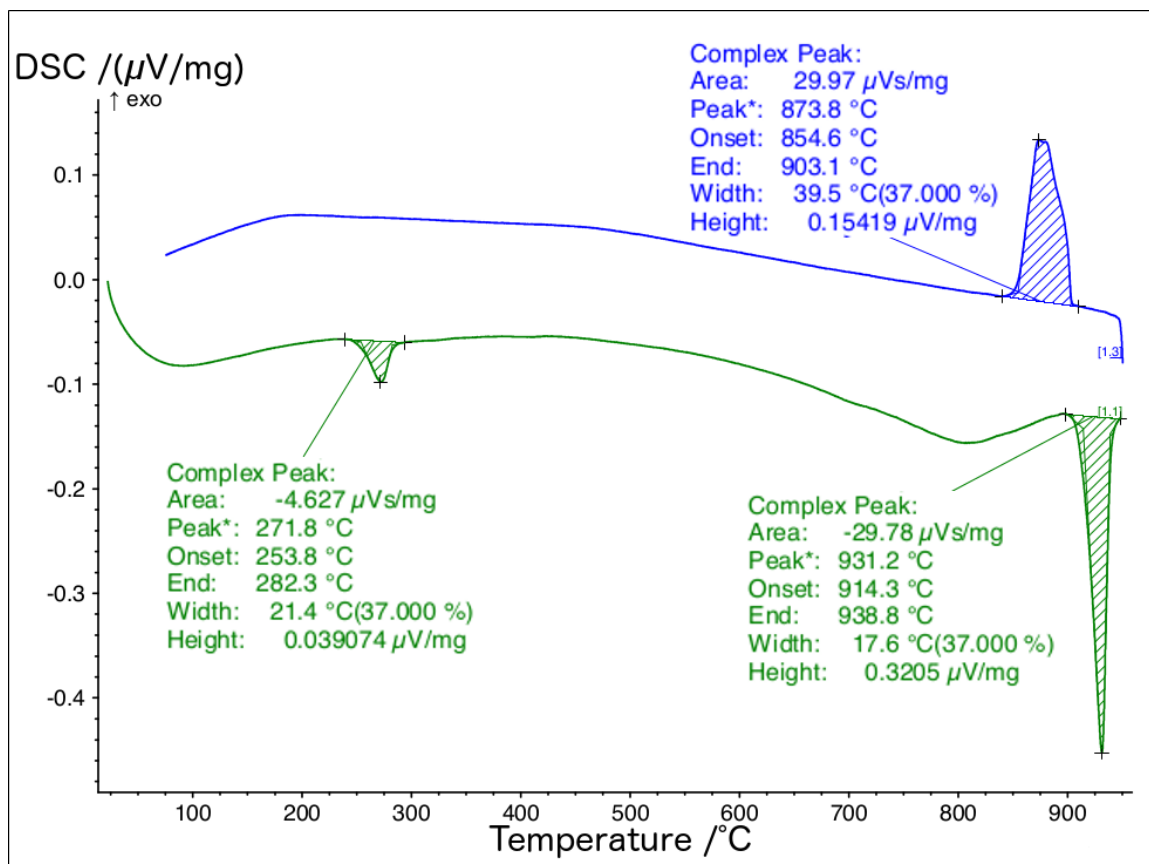


Figure 4.4: First DSC measurement of Pr247 in air. Unidentified low temperature irreversible transition, followed by a broad irreversible peak at 806 (not highlighted), and a high temperature reversible transition.

4.2 $\text{Pr}_2\text{Ba}_4\text{Cu}_7\text{O}_{15-\delta}$ in air

In order to check for other phases, alternate stoichiometries were tested. In particular, $\text{Pr}_2\text{Ba}_4\text{Cu}_7\text{O}_{15-\delta}$ has been reported as superconducting with notably different properties than superconducting Pr123, and with questions around the actual phase synthesized. The question is whether Pr247 and Pr124 are distinct phases with regular structures separate from that of Pr123, or whether they each describe portions of the same incommensurately structured material.

This is backed up by TEM data shown in Chapter 1 from the same group who has claimed distinct synthesis temperatures for Pr247 and Pr124 based on their XRD data. But in Figure 4.4 there is a lack of distinct transitions in air- just one irreversible transition

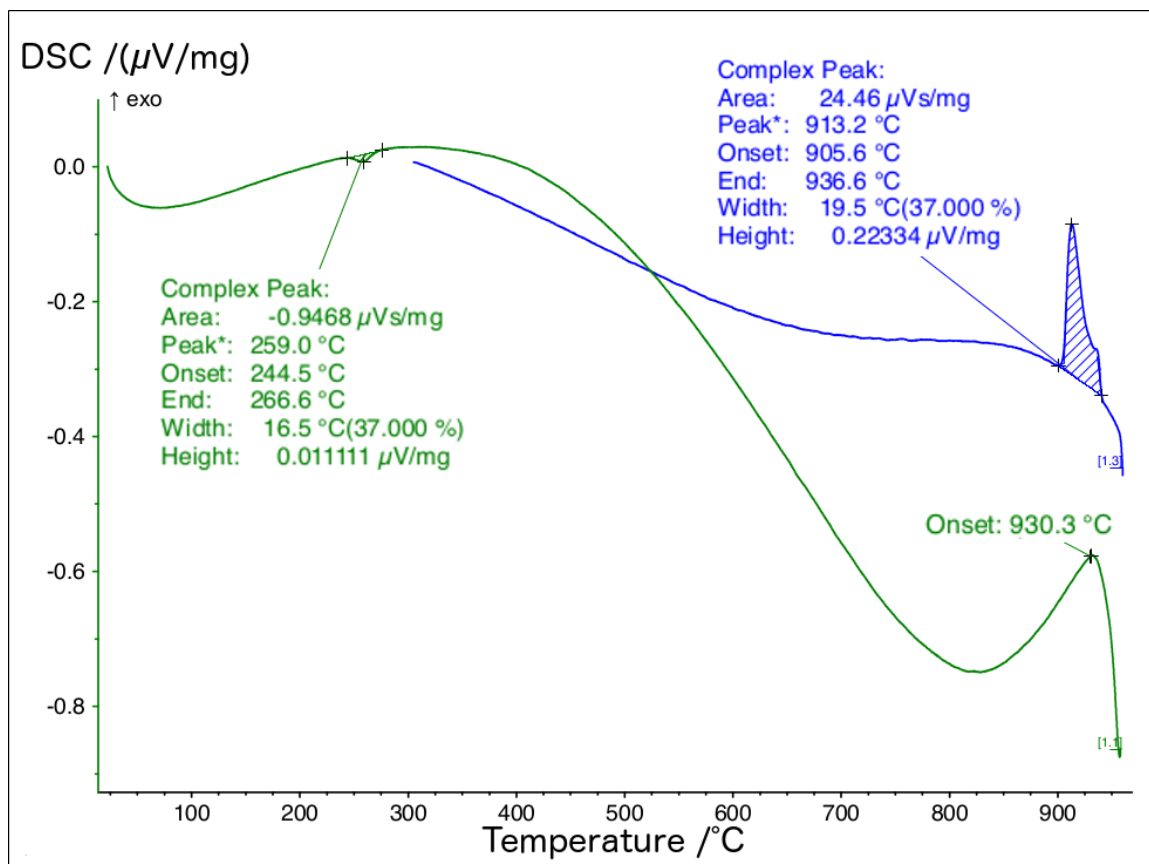


Figure 4.5: Pr247 in flowing oxygen. The overall slope is due to the different thermal characteristics of oxygen changing the baseline. The minimum is around the expected location for the Pr123 formation.

in the expected range which occurs at the same point as the previously witnessed transition for Pr123. Does another transition appear when oxygen is used?

4.3 $\text{Pr}_2\text{Ba}_4\text{Cu}_7\text{O}_{15-\delta}$ in oxygen

No distinct transition is seen in Figure 4.5. As might be expected, the reversible transition of believed to be the partial melting of impurities has increased in temperature due to the oxygen atmosphere. This is most likely the same peak seen in Pr123, though the different chemical composition (additional copper) has altered the dynamics.

Notably, at $5^\circ/\text{min}$ one can make out two distinct transitions at high temperature in Figure 4.6 where only one was evident at full speed, believed to be the two impurity phases.

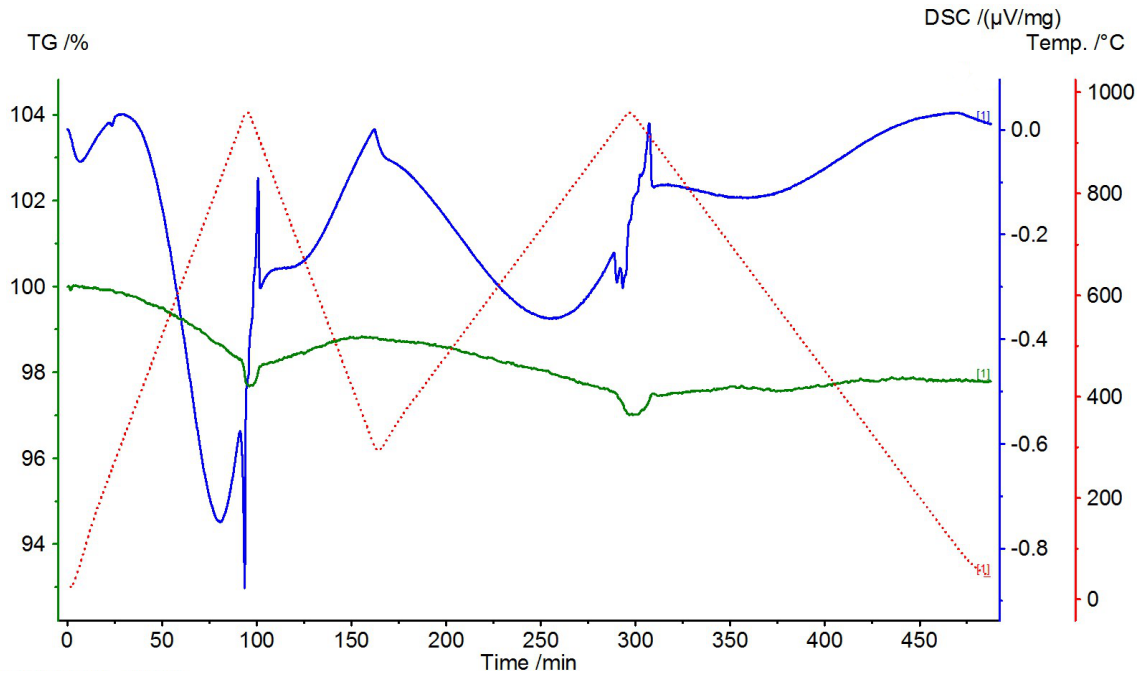


Figure 4.6: Pr247 in flowing oxygen. Full data- DSC and TGA for two consecutive runs at different speeds (10 and 5 degrees Celcius/second). Green line is TGA, blue is DSC, red is temperature.

No such splitting occurs for the primary phase formation, but one can see the oxygen release and re-uptake associated with cuprate melting and reformation.

4.4 $PrBa_2Cu_3O_{7-\delta}$ in reducing atmosphere

Lastly, to check the opposite extreme. It was in argon atmosphere that Luszczek *et al.* [5] conducted the key annealing step, as well as being the standard method for synthesizing R123 compounds to reduce impurities. Thus it is important to measure whether a reducing atmosphere permits the formation of additional phases or significantly changes the reactions taking place. However, no new phase transitions are seen up to 900° C. Instead, witness a characteristic sharpening of the peak identified as the formation temperature of the majority phase, in this case at 834.8° C (Fig. 4.7).

This shape of the peak is indicative both of the polycrystalline sample, lending the shoulders and irregularities, while the large, sharp peak is an indicator of the reaction running more rapidly and efficiently in reducing atmosphere. This re-affirms the conventional

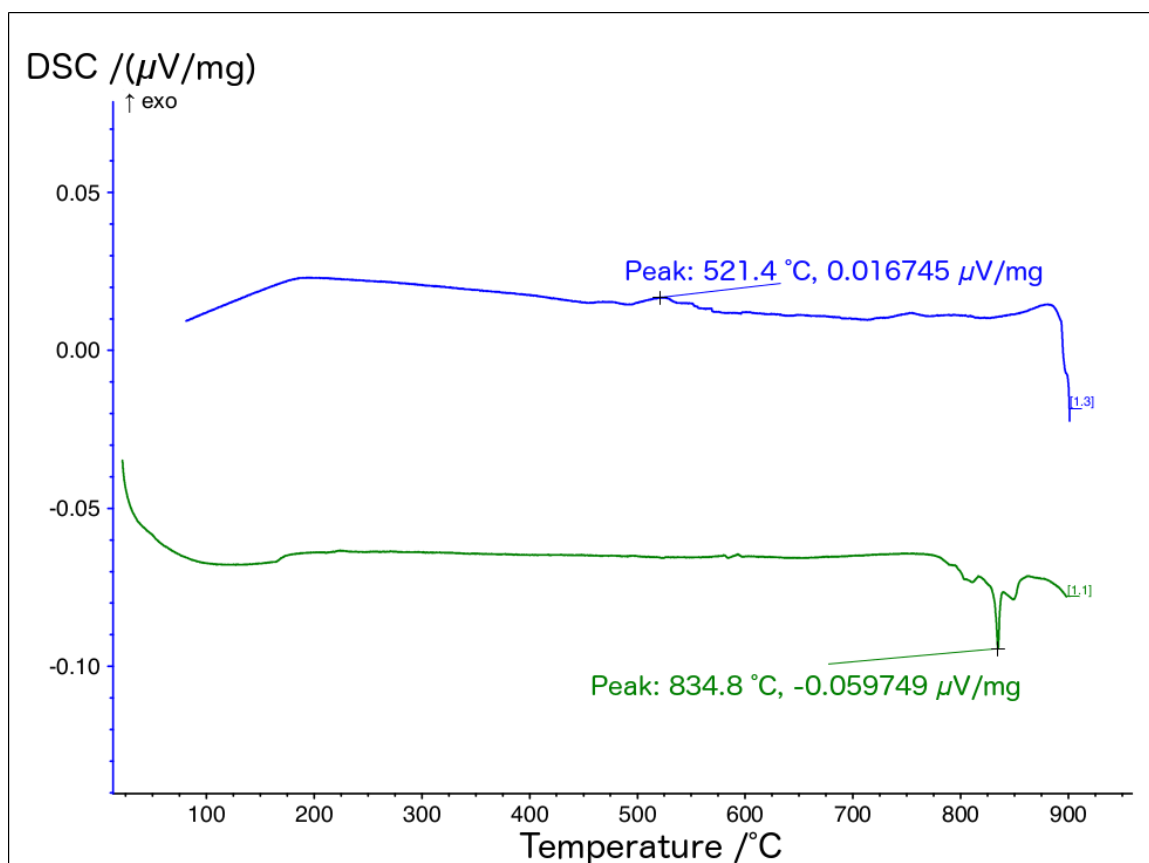


Figure 4.7: DSC measurement for a Pr123 sample in reducing (helium) atmosphere. Shows a clear irreversible transition peaking sharply at 834.8° C, interpreted as the formation of Pr123. The shoulders of the peak are likely due to the polycrystalline nature of the sample.

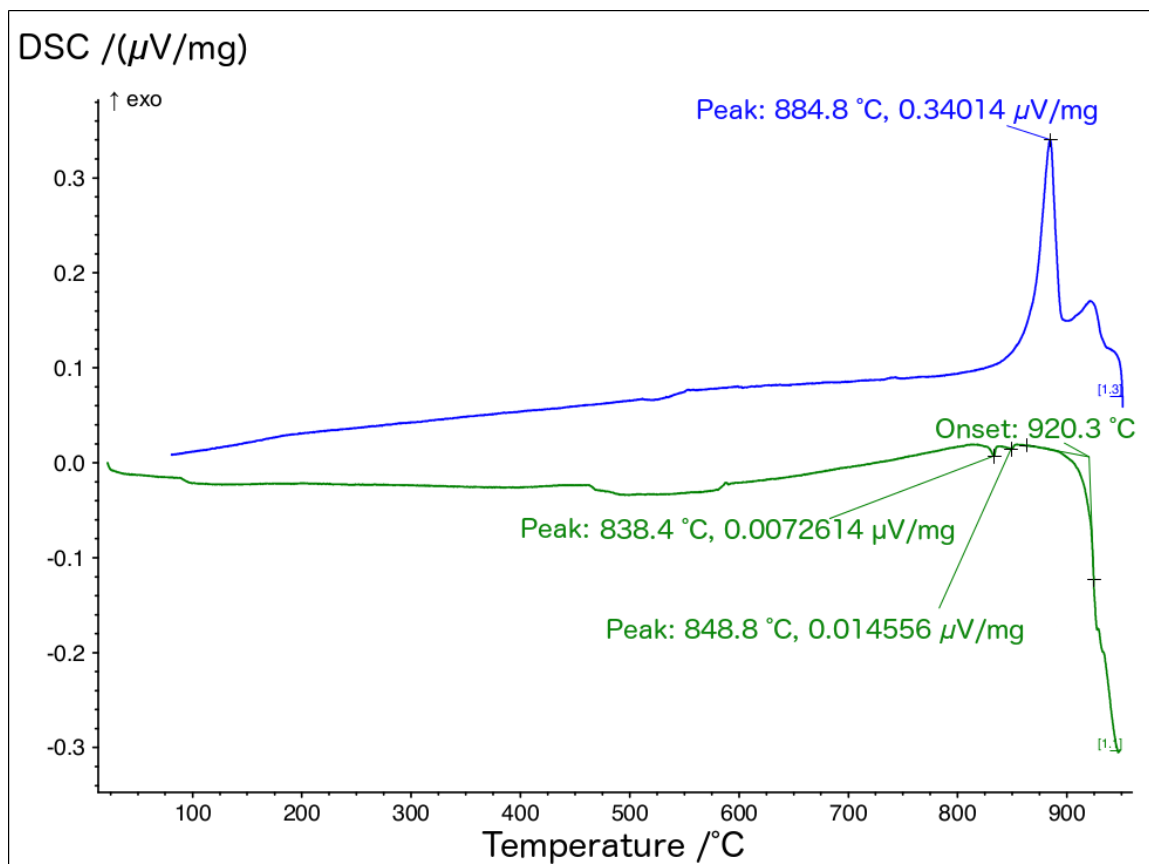


Figure 4.8: DSC measurement for a second piece of the same Pr123 sample in reducing (helium) atmosphere up to 950° C. Demonstrates the lower melting point in reducing atmosphere of 920° C, as compared to 971° C in air.

wisdom around synthesis in reducing atmosphere for the compound. It is unlikely that the shoulders are distinct transitions, such as those for Pr124 and Pr247, as they have been speculated and reported to be at temperatures above 880° C.

By running the same measurement up to 950° C, I can report for the first time the melting point of Pr123 in reducing atmosphere to be $\approx 920^\circ\text{C}$, recrystallizing into what appear to be at least two different phases on cooling (Fig. 4.8). This is below even the lowest temperature (970° C) used by Luszczyk *et al.* [5] for reduction reported to yield superconductivity. While single crystals can be expected to have higher melting points than polycrystalline samples, I judge it likely that their sample exhibited partial melting and re-crystallization into Pr211 and other impurity phases. This is supported in part by the formation of new crystallites on the surface of their single crystals [5].

Chapter 5

Conclusions

What can one learn from all this? Firstly, I have established that the consensus view of $PrBa_2Cu_3O_{7-\delta}$ and $Pr_2Ba_4Cu_7O_{15-\delta}$ is correct. This is not a superconductor, unless it only becomes superconducting under stress/strain captured in a single crystal that is not present in the polycrystalline samples studied here. This would be consistent with many of the published results, in particular the gradual loss of superconductivity in previously superconducting samples as reported in [46, 5]. A pressure study on single crystals would be ideal, however, silence speaks volumes: such studies have likely been done and remained unpublished due to an inability to replicate results.

We have additionally determined that some of the conditions utilized would yield impurity phases rather than Pr123. In particular, high temperature anneals in reducing atmosphere produce Pr211, which while it has exotic magnetic properties, is not superconducting. Instead DC magnetization measurements reveal possible competing local FM and AFM magnetic ordering, and I have eliminated the possibility of it being a spin glass with never before published AC magnetic measurements. Inter-facial or pressure effects are off course possible between the two different magnetic species.

Superconductivity aside, there has long been a presumption in the literature that Pr123, Pr124 and Pr247 are distinct species. The thermal data argues otherwise, failing to show separate transitions or formation temperatures in air or oxygen. In fact, the truth seems to be the simplest possible interpretation of the TEM data, that the crystal structure of

these materials is incommensurate and that there is little order to the stacking of single and double copper oxygen chain containing unit cells [32]. Furthermore, there does not exist a distinct superconducting phase that can be gained from a high temperature thermal treatment- the only transitions in that range are reversible and ascribed to impurity phases.

In fact, the only place where there any evidence of distinct irreversible transitions is found is in reducing atmosphere, but as they are only shoulders on the formation temperature of Pr123 and neither of the other two species has ever been reported to form in reducing atmosphere, that is attributable to the polycrystalline sample. We've also reported for the first time the melting point of polycrystalline Pr123 samples in reducing atmosphere, at around 920° C.

Praseodymium has a complex electronic structure, yielding unique behavior in the cuprates. There is a great deal more to be learned about how this inhibits superconductivity, but this work has allowed us to make two recommendations. One: $PrBa_2Cu_3O_{7-\delta}$ may be safely pursued as an insulating substrate. Two: study the high pressure behavior of both Pr123 and Pr211, with and without aluminum doping, in single crystals if possible. That is the only possible circumstance remaining for superconductivity in the system. Three: for the sake of completeness, synthesize and test the impurity phases to identify exact the nature of the high temperature transitions. If learning the background of the family of compounds has demonstrated anything, it is that there is a great deal the field does not know about the relatively simple ternary oxides.

Bibliography

- [1] Y. Nishihara, Z. Zou, J. Ye, K. Oka, T. Minawa, H. Kawanaka, and H. Bando. Superconducting and non-superconducting $PrBa_2Cu_3O_7$. *Bulletin of Materials Science*, 22(3):257–263, 1999.
- [2] H.B. Radousky. A review of the superconducting and normal state properties of $Y_{1-x}Pr_xBa_2Cu_3O_7$. *Journal of Material Research*, 7(7):1917–1955, 1992.
- [3] H. A. Blackstead, J. D. Dow, D. B. Chrisey, J. S. Horwitz, M. A. Black, P. J. McGinn, A. E. Klunzinger, and D. B. Pulling. Observation of superconductivity in $PrBa_2Cu_3O_7$. *Physical Review B*, 54(9):6122–6125, Sep 1996.
- [4] Z. Zou, K. Oka, T. Ito, and Y. Nishihara. Bulk superconductivity in single crystals of $PrBa_2Cu_3O_{7-x}$. *Japanese Journal of Applied Physics*, 36(Part 2, No. 1A/B):L18–L20, 1997.
- [5] M. Luszczek, W. Sadowski, T. Klimczuk, J. Olchowik, B. Susla, and R. Czajka. Superconductivity in $PrBa_2Cu_3O_{7-\delta}$ single crystals after high-temperature thermal treatment. *Physica C: Superconductivity and its Applications*, 322(1-2):57–64, Sep 1999.
- [6] F. M. Araujo-Moreira, P. N. Lisboa-Filho, S. M. Zanetti, E. R. Leite, and W. A. Ortiz. Superconductivity in sintered-polycrystalline $PrBa_2Cu_3O_{7-\delta}$. *Physica B: Condensed Matter*, 284:1033–1034, 2000.
- [7] M. Hagiwara, T. Shima, T. Sugano, K. Koyama, and M. Matsuura. Ambient pressure synthesis of Pr124 and Pr247 using citrate pyrolysis precursor method. *Physica C: Superconductivity and its Applications*, 445-448:111–114, Oct 2006.

- [8] J. Ye, Z. Zou, K. Oka, Y. Nishihara, A. Matsushita, and T. Matsumoto. Superconducting and structural properties of $PrBa_2Cu_3O_x$ under high pressure. *Physica B: Condensed Matter*, 259:533–535, Jan 1999.
- [9] C. Stari, L. Cichetto, C. H. M. A. Peres, V. A. G. Rivera, S. Sergeenkov, C. A. Cardoso, E. Marega, and Araújo-Moreira, F. M. Comparative study on structure and magnetic properties of polycrystalline $Pr_xY_{1-x}Ba_2Cu_3O_{7-\delta}$ prepared in oxygen and argon atmosphere. *Journal of Alloys and Compounds*, 528:135–140, 2012.
- [10] V. Ghanbarian and M. R. Mohammadzadeh. Different self-consistent electronic structures of $PrBa_2Cu_3O_7$ from LSDA+U calculations. *Physical Review B*, 78(14), 2008.
- [11] L. Soderholm, M. A. Beno, J. D. Jorgensen, C. U. Segre, and I. K. Schuller. Incorporation of Pr in $YBa_2Cu_3O_{7-\delta}$: electronic effects on superconductivity. *Nature*, 328(6131):604–605, 1987.
- [12] C.T. Lin, J. Chrosch, , W.Y. Liang, and E.K.H. Salje. Superconducting YBCO single crystals with macroscopically tetragonal phase. *Physica C: Superconductivity and its Applications*, 242(1-2):105–112, Feb 1995.
- [13] J. D. Jorgensen, M. A. Beno, D. G. Hinks, L. Soderholm, K. J. Volin, R. L. Hitterman, J. D. Grace, I. K. Schuller, C. U. Segre, K. Zhang, and M. S. Kleefisch. Oxygen ordering and the orthorhombic-to-tetragonal phase transition in $YBa_2Cu_3O_{7-x}$. *Physical Review B*, 36(7):3608–3616, Sep 1987.
- [14] S. Subramanian, C. S. Swamy, and H. G. Karge. Formation of a new superconducting tetragonal phase, YBCO-T* ($T_c = 87$ K) in $YBa_2Cu_3O_{7-\delta}$. *Journal of Materials Science Letters*, 12(12):928–931, 1993.
- [15] R. M. Hazen, L. W. Finger, R. J. Angel, C. T. Prewitt, N. L. Ross, H. K. Mao, C. G. Hadidiacos, P. H. Hor, R. L. Meng, and C. W. Chu. Crystallographic description of phases in the Y-Ba-Cu-O superconductor. *Physical Review B*, 35(13):7238–7241, may 1987.

- [16] A. Kebede, C. S. Jee, J. Schwegler, J. E. Crow, T. Mihalisin, G. H. Myer, R. E. Salomon, P. Schlottmann, M. V. Kuric, S. H. Bloom, and R. P. Guertin. Magnetic ordering and superconductivity in $Y_{1-x}Pr_xBa_2Cu_3O_{7-y}$. *Physical Review B*, 40(7):4453–4462, Sep 1989.
- [17] G. Nieva, S. Ghamaty, B. W. Lee, M. B. Maple, and I. K. Schuller. Superconductivity and magnetism in $Eu_{1-x}Pr_xBa_2Cu_3O_{7-\delta}$. *Physical Review B*, 44(13):6999–7007, 1991.
- [18] B. Okai, K. Takahashi, H. Nozaki, M. Saeki, M. Kosuge, and M. Ohta. Preparation and physical properties of $PrBa_2Cu_3O_y$. *Japanese Journal of Applied Physics*, 26(Part 2, No. 10):L1648–L1650, Oct 1987.
- [19] L Soderholm, C.-K. Loong, GL Goodman, and BD Dabrowski. Crystal-field splittings and magnetic properties of Pr^{3+} and Nd^{3+} in $RBa_2Cu_3O_7$. *Physical Review B*, 43(10):7923–7935, Apr 1991.
- [20] Y. Takano, S. Yokoyama, K. Kanno, and K. Sekizawa. The paramagnetic susceptibility of $PrBa_2Cu_3O_7$. *Physica C: Superconductivity and its Applications*, 252(1-2):61–66, Oct 1995.
- [21] H. D. Yang, P. F. Chen, C. R. Hsu, C. W. Lee, C. L. Li, and C. C. Peng. Suppression of superconductivity in $Gd_{1-x}Pr_xBa_2Cu_3O_{7-y}$ and $R_{0.8}Pr_{0.2}Ba_2Cu_3O_{7-y}$ systems. *Physical Review B*, 43(13):10568–10573, May 1991.
- [22] H. D. Yang and M. W. Lin. Effects of Zn and Ga substitution on the magnetic properties of $PrBa_2Cu_3O_{7-y}$. *Physical Review B*, 44(10):5384–5387, Sep 1991.
- [23] D. P. Norton, D. H. Lowndes, B. C. Sales, J. D. Budai, B. C. Chakoumakos, and H. R. Kerchner. Superconductivity and hole doping in $Pr_{0.5}Ca_{0.5}Ba_2Cu_3O_{7-\delta}$ thin films. *Physical Review Letters*, 66(11):1537, Mar 1991.
- [24] F.M. Araujo-Moreira, P.N. Lisboa-Filho, A.J.C. Lanfredi, W.A. Ortiz, S.M. Zanetti, E.R. Leite, A.W. Mombrú, L Ghivelder, Y.G. Zhao, and V. Venkatesan. The search

- for superconductivity in $PrBa_2Cu_3O_{7-\delta}$. *Physica C: Superconductivity and its Applications*, 341-348:413–416, Nov 2000.
- [25] M.E. López-Morales, D. Ríos-Jara, J. Tagüea, R. Escudero, S. La Placa, A. Bezinge, V. Y. Lee, E. M. Engler, and P.M. Grant. Role of oxygen in $PrBa_2Cu_3O_{7-y}$: Effect on structural and physical properties. *Physical Review B*, 41(10):6655–6667, 1990.
- [26] J. Ye, Z. Zou, K. Oka, Y. Nishihara, and T. Matsumoto. Possible origins of superconductivity in $PrBa_2Cu_3O_x$ compound viewed from results of single crystal structure study. *Journal of Alloys and Compounds*, 288(1-2):319–325, 1999.
- [27] S. Horii, Y. Yamada, H. Ikuta, N. Yamada, Y. Kodama, S. Katano, Y. Funahashi, S. Morii, A. Matsushita, T. Matsumoto, I. Hirabayashi, and U. Mizutani. Synthesis and superconducting properties of $(Y_{1-x}Pr_x)Ba_2Cu_4O_8$ and $(Y_{1-x}Pr_x)_2Ba_4Cu_7O_{15-y}$ compounds. *Physica C: Superconductivity and its Applications*, 302(1):10–22, Jun 1998.
- [28] H. D. Yang, J.-Y. Lin, S. S. Weng, C. W. Lin, H. L. Tsay, Y. C. Chen, T. H. Meen, T. I. Hsu, and H. C. Ku. Magnetic ordering and transport properties of $PrBa_2Cu_4O_8$. *Physical Review B*, 56(21):14180–14184, Dec 1997.
- [29] M. Kakihana, S. Kato, V. Petrykin, J. Bäckström, L. Börjesson, and M. Osada. A simple and reproducible way to synthesize $PrBa_2Cu_4O_8$ under 1 atm of oxygen by amorphous citrate method. *Physica C: Superconductivity and its Applications*, 321(1-2):74–80, Aug 1999.
- [30] C.W. Lin, J.-Y. Lin, H.D. Yang, T.H. Meen, H.L. Tsay, Y.C. Chen, J.C. Huang, S.R. Sheen, and M.K. Wu. Synthesis of $PrBa_2Cu_4O_8$ at ambient oxygen pressure. *Physica C: Superconductivity and its Applications*, 276(3-4):225–228, Mar 1997.
- [31] M. Kuwabara, M. Matsukawa, K. Sugawara, H. Taniguchi, A. Matsushita, Makoto Hagiwara, Kazuhiro Sano, Yoshiaki Ōno, and Takahiko Sasaki. Effect of pressure on magneto-transport properties in the superconducting and normal phases of the metallic double chain compound $Pr_2Ba_4Cu_7O_{15-\delta}$. *Journal of the Physical Society of Japan*, 85(12):124704, Dec 2016.

- [32] M. Hagiwara, T. Shima, S. Tanaka, K. Nishio, T. Isshiki, T. Saito, and K. Koyama. Superconductivity and structural characteristics of ceramic $Pr_2Ba_4Cu_7O_{15-\delta}$ prepared by ambient pressure synthesis using citrate pyrolysis method. *Physica C: Superconductivity and its Applications*, 463-465:161–164, Oct 2007.
- [33] Toshiyuki Usagawa, Yoshihiro Ishimaru, Jianguo Wen, Tadashi Utagawa, Satoshi Koyama, and Youichi Enomoto. Superconductivity in (110) $PrBa_2Cu_3O_{7-\delta}$ thin films pseudomorphically grown on (110) $YBa_2Cu_3O_{7-\delta}$ single crystal substrates. *Japanese Journal of Applied Physics*, 36(Part 2, No. 12A):L1583–L1586, Dec 1997.
- [34] W. L. Hults, J. C. Cooley, E. J. Peterson, J. L. Smith, H. A. Blackstead, and J. D. Dow. $PrBa_2Cu_3O_{7-x}$ polycrystalline superconductor preparation. *International Journal of Modern Physics B*, 12(29n31):3278–3283, Dec 1998.
- [35] HA Blackstead and JD Dow. Implications of superconductivity of $PrBa_2Cu_3O_7$. *Solid State Communications*, 115(3):137–140, Jun 2000.
- [36] S. A. Hodorowicz, W. Lasocha, A. Lasocha, and H. A. Eick. The preparation and magnetic behavior of $EuBa_2Cu_{3-y}M_yO_{6.5+x}$ (M = Ni, Co, Al, and Zn) and some related compounds. *Journal of Solid State Chemistry*, 77(1):148–155, nov 1988.
- [37] Z. Zou, J. Ye, K. Oka, and Y. Nishihara. Superconducting $PrBa_2Cu_3O_x$. *Phys. Rev. Lett.*, 80(5):1074–1077, 1998.
- [38] Kunihiko Oka, Zhigang Zou, and Jinhua Ye. Crystal growth of superconductive $PrBa_2Cu_3O_{7-y}$. *Phys C Supercond*, 300(3-4):200–206, 1998.
- [39] John D Dow and Dale R Harshman. Explanation of high-temperature superconductivity without cuprate planes. *Philosophical Magazine B*, 82(9):1055–1066, Jun 2002.
- [40] J. D. Dow and D. R. Harshman. BaO planes, not CuO_2 planes, contain high-TC superconductivity. *International Journal of Modern Physics B*, 21(18n19):3086–3095, jul 2007.

- [41] II Mazin and AI Liechtenstein. Location of holes in $Y_{1-x}Pr_xBa_2Cu_3O_7$. *Physical Review B*, 57(1):150–152, Jan 1998.
- [42] II Mazin. Theoretical possibilities for superconductivity in $PrBa_2Cu_3O_7$. *Physical Review B*, 60(1):92–95, Jul 1999.
- [43] R Fehrenbacher and TM Rice. Unusual electronic structure of $PrBa_2Cu_3O_7$. *Physical Review Letters*, 70(22):3471–3474, May 1993.
- [44] V. N. Narozhnyi and S.-L. Drechsler. Comment on “Superconducting $PrBa_2Cu_3O_x$ ”. *Physical Review Letters*, 82(2):461–461, Jan 1999.
- [45] W. Widder, M. Stebani, L. Bauernfeind, H.F. Braun, K. Widder, H.P. Geserich, M. Rbhausen, N. Dieckmann, and A. Bock. Growth and characterization of (Y, Pr)-123 single crystals: influence of Al contamination and post-annealing under oxygen pressure. *Physica C: Superconductivity and its Applications*, 256(1-2):168–176, Jan 1996.
- [46] M. Luszczek and W. Sadowski. Surface morphology of $PrBa_2Cu_3O_{7-\delta}$ single crystals after the long-lasting high-temperature reduction. *Open Physics*, 1(4), Jan 2003.
- [47] T. Konno, M. Matsukawa, K. Sugawara, H. Taniguchi, J. Echigoya, A. Matsushita, M. Hagiwara, K. Sano, Y. Ohno, Y. Yamada, T. Sasaki, and Y. Hayasaka. Thermodynamic properties of superconducting and non-superconducting $Pr_2Ba_4Cu_7O_{15-\delta}$ compounds with metallic double chains. *Physica C: Superconductivity and its Applications*, 521-522:13–17, Feb 2016.
- [48] T. Itoh, K. Kitazawa, and S. Tanaka. Specific heat and superconductivity in $BaPb_{1-x}Bi_xO_3$. *Journal of the Physical Society of Japan*, 53(8):2668–2673, Aug 1984.
- [49] C. Infante, M.K. El Mously, R. Dayal, M. Husain, S.A. Siddiqi, and P. Ganguly. On the localisation of charge carriers and suppression of superconductivity by praseodymium in systems derived from $YBa_2Cu_3O_{7-d}$. *Physica C: Superconductivity and its Applications*, 167(5-6):640–656, May 1990.

- [50] H.D. Yang, M.W. Lin, C.H. Luo, H.L. Tsay, and T.F. Young. Effects of ca substitution on the structural, electrical and magnetic properties of $PrBa_2Cu_3O_{7-y}$. *Physica C: Superconductivity and its Applications*, 203(3-4):320–326, Dec 1992.
- [51] M. Luszczek and R. Laskowski. The influence of Pr/Ba disorder on the electronic structure of $PrBa_2Cu_3O_7$. *Physica Status Solidi (b)*, 230(2):R1–R3, Apr 2002.
- [52] Y. G. Zhao, S. Y. Xiong, Y. P. Li, B. Zhang, S. S. Fan, B. Yin, J. W. Li, S. Q. Guo, W. H. Tang, G. H. Rao, D. J. Dong, B. S. Cao, and B. L. Gu. Structural, transport, and magnetic properties of $PrBa_{2-x}Sr_xCu_3O_{7-\delta}$. *Physical Review B*, 56(14):9153–9157, Oct 1997.
- [53] Y. G. Zhao, Z. W. Dong, M. Rajeswari, R. P. Sharma, and T. Venkatesan. Growth of single-phase $PrBa_{0.7}Sr_{1.3}Cu_3O_7$ thin films and the role of lattice strain on the transport properties. *Applied Physics Letters*, 72(8):981–983, Feb 1998.
- [54] Y. G. Zhao, Z. W. Dong, M. Rajeswari, R. P. Sharma, and T. Venkatesan. Electrical transport properties of highly doped $PrBa_{2-x}Sr_xCu_3O_7$ thin films prepared by pulsed laser deposition. *Physical Review B*, 58(2):1068–1072, Jul 1998.
- [55] Y.G. Zhao, M. Rajeswari, R.C. Srivastava, Z.W. Dong, R.P. Sharma, and T. Venkatesan. Growth and electrical properties of $PrSr_2Cu_3O_{7-\delta}$ thin films. *Physica C: Superconductivity and its Applications*, 328(3-4):152–156, Dec 1999.
- [56] V.P.S. Awana, M.A. Ansari, Anurag Gupta, R.B. Saxena, H Kishan, Rajeev Rawat, V Ganesan, A.V. Narlikar, Devendra Buddhikot, and S.K. Malik. Induction of superconductivity in $Y_{0.4}Pr_{0.6}Ba_{2x}Sr_xCu_3O_7$ system with increasing Sr substitution. *Physica C: Superconductivity and its Applications*, 417(1-2):33–39, 2004.
- [57] D. P. Norton, D. H. Lowndes, B. C. Sales, J. D. Budai, E. C. Jones, and B. C. Chakoumakos. Transport and structural properties of $Pr_{1-x}Ca_xBa_2Cu_3O_{7-\delta}$ thin films grown by pulsed-laser deposition. *Physical Review B*, 49(6):4182–4188, Feb 1994.

- [58] M Akhavan. Ba@Pr or Pr@Ba in R123 HTSC to be or not to be SC. *Physica Status Solidi (b)*, 241(6):1242–1250, 2004.
- [59] H.D. Yang, I.P. Hong, S. Chatterjee, P. Nachimuthu, J.M. Chen, and J.-Y. Lin. X-ray absorption near-edge structure of $Pr_{1-x}Ba_{2+x}Cu_3O_7$. *Physica C: Superconductivity and its Applications*, 341-348:411–412, Nov 2000.
- [60] K. Rogacki, B. Dabrowski, and O. Chmaissem. Increase of critical currents and peak effect in Mo-substituted $YBa_2Cu_3O_7$. *Physical Review B*, 73(22), Jun 2006.
- [61] HL Tsay, YC Chen, FL Juang, WM Wang, and HD Yang. Occurrence of superconductivity in Ca- and Sr -doped $PrSr_2Cu_{2.7}Mo_{0.3}O_{7-\delta}$. *Physical Review B*, 53(17):11340–11343, May 1996.
- [62] H. D. Yang, H. L. Tsay, C. R. Shih, and Y. C. Chen. Superconductivity and magnetism in $Y_{1-x}Pr_xSr_2Cu_{2.7}Mo_{0.3}O_{7-\delta}$. *Physical Review B*, 51(13):8543–8550, Apr 1995.
- [63] Li, Chang, Hsieh, Lee, Lynn, and Yang. Magnetic ordering of Pr in $PrBa_2Cu_{2.7}Zn_{0.3}O_{7-y}$. *Physical Review B*, 48(1):519–523, Jul 1993.
- [64] Y.G. Zhao, S.L. Jia, Y.Q. Zhou, Y. Yang, and Z.X. Zhao. Effect of Zn doping on Tc of $Y_{1-x}Pr_xBa_2Cu_{3-y}Zn_yO_z$ and its dependence on Pr doping. *Physica C: Superconductivity and its Applications*, 209(4):472–476, May 1993.
- [65] H. D. Yang, H. L. Tsay, C. R. Shih, T. H. Meen, and Y. C. Chen. Magnetic-field effect on the specific heat of $PrBa_2(Cu_{1-x}Ga_x)_3O_{7-\delta}$. *Physical Review B*, 52(21):15099–15102, Dec 1995.
- [66] S. Uma, G. Rangarajan, and E. Gmelin. Influence of Al substitution in $PrBa_2Cu_3O_{7-\delta}$ single crystals. *Physica C: Superconductivity*, 301(3-4):141–146, Jun 1998.
- [67] K. Widder, M. Merz, D. Berner, J. Mnzal, H.P. Geserich, A. Erb, R. Flkiger, W. Widder, and H.F. Braun. Optical investigation of $Y_{1-z}Pr_zBa_2Cu_3O_{7-\delta}$ single-domain crystals. a comparison between impurity-free and Al doped samples. *Physica C: Superconductivity and its Applications*, 264(1-2):11–18, Jun 1996.

- [68] M. Łuszczek and W. Sadowski. Growth and electric transport of Ca-doped $PrBa_2Cu_3O_{7-\delta}$ single crystals. *Crystal Research and Technology*, 36(8-10):917–923, Oct 2001.
- [69] P. N. Lisboa-Filho, S. M. Zanetti, A. W. Mombrú, P. A. P. Nascente, E. R. Leite, W. A. Ortiz, and Araújo-Moreira, F. M. Crystallographic, microstructural and magnetic properties of polycrystalline $PrBa_2Cu_3O_{7-\delta}$. *Superconductor Science and Technology*, 14(8):522, 2001.
- [70] J. Shi, J.E. Berger, and X.S. Ling. Growth of $YBa_2Cu_3O_7$ -crystals with $BaZrO_3$ -coated alumina crucibles. *Physica C: Superconductivity and its Applications*, 301(3-4):215–220, Jun 1998.
- [71] Netzsch. *Netzsch STA 449 F1 Jupiter[®] Technical Specifications*.
- [72] Jack W. Ekin. *Experimental Techniques for Low-Temperature Measurements*. Oxford University Press, 2006.
- [73] Z. Zhu, D. Gao, J. Zhang, Z. Shi, H. Gao, Z. Yang, Z. Zhang, and D. Xue. Coexistence of ferromagnetism and spin glass behavior in antiferromagnetic Y_2BaCuO_5 . *Physica C: Superconductivity and its Applications*, 490:32–36, Jul 2013.
- [74] E. D. Dahlberg, M. Hardiman, R. Orbach, and J. Souletie. High-frequency ac susceptibility and ESR of a spin-glass. *Physical Review Letters*, 42(6):401–404, Feb 1979.
- [75] J.L. Tholence. On the frequency dependence of the transition temperature in spin glasses. *Solid State Communications*, 35(2):113–117, Jul 1980.
- [76] M. Hagiwara, S. Tanaka, T. Shima, K. Gotoh, S. Kanda, T. Saito, and K. Koyama. Superconductivity of reduction-treated ceramic material of $Pr_2Ba_4Cu_7O_{15-\delta}$ mixed with the related structure phases. *Physica C: Superconductivity and its Applications*, 468(15-20):1217–1220, Sep 2008.

- [77] H.-J. Chen and J. H. Sharp. An investigation into the self-propagating high temperature synthesis (SHS) of superconducting ceramics by thermal methods. *Journal of Thermal Analysis*, 40(1):379–386, jul 1993.